ACCEPTED MANUSCRIPT

Journal of Vacuum Science & Technology A

This is the author's peer reviewed, accepted manuscript. However, the online version of record will be different from this version once it has been copyedited and typeset.
PLEASE CITE THIS ARTICLE AS DOI: 10.1116/6.0002115

Growth and characterization of α-Ga_2O_3 on sapphire and nanocrystalline β-Ga_2O_3 on diamond substrates by halide vapor phase epitaxy

Sushrut Modak[1], James Spencer Lundh[2,3], Nahid Sultan Al-Mamun[4], Leonid Chernyak[1], Aman Haque[4], Thieu Quang Tu[5], Akito Kuramata[5], Marko J. Tadjer[2], Stephen J. Pearton[6]

[1]Department of Physics, University of Central Florida, Orlando, FL 32816, USA

[2]U.S. Naval Research Laboratory, Washington, DC 20375

[3]National Research Council Research Associateship Programs, Washington, DC 20001

[4]Mechanical Engineering, The Pennsylvania State University, University Park, PA 16802

[5]Novel Crystal Technology, Sayama-city, Saitama, Japan

[6]Department of Materials Science and Engineering, University of Florida, Gainesville, FL 32611, USA

Corresponding Author: marko.tadjer@nrl.navy.mil

Abstract

Halide vapor phase epitaxial (HVPE) Ga_2O_3 films were grown on c-plane sapphire and diamond substrates at temperatures up to 550 °C without the use of a barrier dielectric layer to protect the diamond surface. Corundum phase α-Ga_2O_3 was grown on the sapphire substrates, whereas the growth on diamond resulted in regions of nanocrystalline β-Ga_2O_3 (nc-β-Ga_2O_3) when oxygen was present in the HVPE reactor only during film growth. X-ray diffraction confirmed the growth of α-Ga_2O_3 on sapphire but failed to detect any β-Ga_2O_3 reflections from the films grown on diamond. These films were further characterized via Raman spectroscopy, which revealed the β-Ga_2O_3 phase of these films. Transmission electron microscopy demonstrated the nanocrystalline character of these films. From cathodoluminescence spectra, three emission bands, UVL′, UVL, and BL, were observed for both the α-Ga_2O_3/sapphire and nc-Ga_2O_3/diamond, and these bands were centered at approximately 3.7 eV, 3.2 eV, and 2.7 eV.

ACCEPTED MANUSCRIPT

Journal of Vacuum Science & Technology A

This is the author's peer reviewed, accepted manuscript. However, the online version of record will be different from this version once it has been copyedited and typeset.
PLEASE CITE THIS ARTICLE AS DOI: 10.1116/6.0002115

Introduction

Gallium oxide (Ga_2O_3) is an attractive material for power electronics due to its ultra-wide bandgap (4.6-4.9 eV), which gives rise to a very high critical electric field (6-8 MV/cm) [1,2]. Significant efforts to develop this material into a technological platform for high-power, fast-switching electronic devices has brought together crystal growth, epitaxial film development, materials scientists, and electronic device researchers over recent years [3,4]. Recent developments have resulted in large-area substrates and epitaxial wafers, lateral transistors with high breakdown voltage in the 6-8 kV range [5,6], and vertical transistor architectures such as the fin field-effect transistor (FinFET) and current aperture vertical electron transistor (CAVET) that show exceptional promise for next-generation power electronics [7–9].

Two challenges persist, however: the ultra-low thermal conductivity of Ga_2O_3 and the impossibility of generating free hole carriers in this material due to self-trapping [10–12]. The low thermal conductivity of Ga_2O_3 could potentially hamper the development of this technology as it limits device power-handling capabilities. To this end, various experiments have been reported in search of improving the prospects of thermal performance of Ga_2O_3. This includes heteroepitaxial growth and wafer bonding of Ga_2O_3 to high thermal conductivity substrates, such as SiC and diamond, as well as capping with a high thermal conductivity material, such as AlN [13–25]. All of these approaches present unique challenges; heteroepitaxial growth in particular presents unique challenges for Ga_2O_3 crystallinity control and phonon matching arising from significant mismatch in lattice constants, coefficients of thermal expansion, phase stability, and phonon density of states[26,27]. Nevertheless, the wide availability of Ga_2O_3 epitaxial growth methods justify further experimentation in this direction.

A previous report by Polyakov et al. demonstrated halide vapor phase epitaxy (HVPE) growth of Ga_2O_3 utilizing an Al_2O_3 interlayer deposited on the diamond surface in order to suppress etching of the diamond surface in the oxygen-rich atmosphere in the HVPE reactor [20]. In this paper, we report HVPE growth of

ACCEPTED MANUSCRIPT
Journal of Vacuum Science & Technology A
This is the author's peer reviewed, accepted manuscript. However, the online version of record will be different from this version once it has been copyedited and typeset.
PLEASE CITE THIS ARTICLE AS DOI: 10.1116/6.0002115

Ga_2O_3 on sapphire and diamond substrates without the use of any barrier dielectric layers. The growth of nanocrystalline Ga_2O_3 (nc-Ga_2O_3) films containing regions of continuous β-Ga_2O_3 on diamond in the absence of a protective barrier dielectric layer was accomplished using N_2 atmosphere during reactor temperature ramp-up. This approach was similar to the one undertaken by Karim et al., where β-Ga_2O_3 films were deposited on diamond via low-pressure chemical vapor deposition (LPCVD) at 900-920 °C after purging the growth chamber in Ar for 1 hour, withholding O_2 until the growth temperature was reached, and growing at lower temperature (750 °C) for the initial 3 minutes of growth [18]. However, in the current experiment, the growth temperature was kept at or below 550 °C. In the succeeding sections, we present detailed structural characterization of the Ga_2O_3 films obtained and suggest future research directions for subsequent experiments.

Experimental Details

X-ray diffraction (XRD) analysis of the commercial CVD single-crystalline (111) diamond substrates used for Ga_2O_3 growth was performed using a Rigaku diffractometer. High resolution symmetric and asymmetric XRD scans were performed to measure in-plane and out-of-plane lattice constants. The lattice constant was measured to be 3.567Å and a 4° offcut from the normal axis towards (100) was determined. The full width at half maximum of the (004) reflection was 144 arcsec. The Ga_2O_3 epitaxial films were grown via HVPE on either c-plane sapphire (c-Al_2O_3) or diamond substrates obtained from Element Six. The GaCl precursor partial pressure (P_{GaCl}) was 3.6×10^{-3} atm for growth on c-Al_2O_3. In order to preserve the diamond surface from decomposition during oxide growth, the growth temperature (T_{Growth}) was limited to a range of 450-550 °C (Table I). Furthermore, temperature ramp-up in the HVPE reactor was performed in the absence of O_2 (only N_2 ambient) in order to suppress etching of the diamond surface at the initiation of film growth. Finally, P_{GaCl} was increased to 5.8×10^{-3} atm via the Cl_2 gas flow rate as initial Ga_2O_3 growth was expected to further protect the diamond surface. The growth time on all samples was 1 hour.

ACCEPTED MANUSCRIPT
Journal of Vacuum Science & Technology A
This is the author's peer reviewed, accepted manuscript. However, the online version of record will be different from this version once it has been copyedited and typeset.
PLEASE CITE THIS ARTICLE AS DOI: 10.1116/6.0002115

Table I – Summary of Ga_2O_3 films grown on c-plane sapphire and diamond substrates in this work.

Sample	Substrate	T_{Growth} (°C)	Ramp-up atmosphere	Input P_{GaCl} (atm)	Thickness from TEM (nm)	5×5 µm AFM rms roughness (nm)
S1	c-Al_2O_3	450	N_2/O_2	3.60×10^{-3}	90	28.9
S2	c-Al_2O_3	500	N_2/O_2	3.60×10^{-3}	140	3.13
S3	Diamond	500	N_2	5.80×10^{-3}	270	27.7
S4	Diamond	550	N_2	5.80×10^{-3}	60	6.04

Atomic force microscopy (AFM) images were obtained using a Bruker Dimension FastScan atomic force microscope. Raman spectroscopy was performed using a Thermo Scientific DXRxi Raman mapping instrument in a $Z(XX)\bar{Z}$ backscattering geometry with a 532 nm excitation wavelength (100X objective, 25 µm confocal hole, 10 mW laser power). Cross-sectional electron transparent (~100 nm thick) samples were prepared for transmission electron microscopy (TEM) study via in-situ lift-out method using the FEI Helios Nanolab 660 dual beam focused ion beam (FIB) system. The cross-sectional TEM bright field images, selected area electron diffraction (SAED) patterns, and nano-diffraction patterns of the TEM samples were acquired using the FEI Talos F200X scanning(S)/TEM system at 200 kV. Cathodoluminescence (CL) from the samples was measured in the temperature range of 77 K – 307 K in an Attolight Allallin 4027 Chronos SEM fitted with a stage with a temperature-controller (CryoVac TIC 500). The samples were excited with an electron beam with an electron energy of 3 keV, which correlates to a Gruen electron range of 46 nm in α-Ga_2O_3. The CL emission is collected with a mirror assembly spatially coupled to a spectrometer (Horiba iHR 320). CL spectra were recorded on a CCD camera (Andor Newton 920p, 180-1100 nm) after the CL emission was dispersed from a grating with 150 grooves/mm blazed at 500 nm within the spectrometer.

Results and Discussion

We first examined the surface quality of the Ga_2O_3 films deposited on sapphire and diamond substrates. AFM imaging of samples S1-S4 (Fig. 1) revealed grains on the surface of all four samples. Root mean square (rms) analysis of these 5 µm × 5 µm scans showed that the roughness improved significantly when the growth temperature was increased. For samples S1 and S2 (Ga_2O_3/sapphire, Figs. 1a and 1b), rms roughness improved from 28.9 to 3.13 nm when the growth temperature was increased from 450 °C to 500

ACCEPTED MANUSCRIPT
Journal of Vacuum Science & Technology A
This is the author's peer reviewed, accepted manuscript. However, the online version of record will be different from this version once it has been copyedited and typeset.
PLEASE CITE THIS ARTICLE AS DOI: 10.1116/6.0002115

°C. Similarly, for samples S3 and S4 (Ga_2O_3/diamond, Figs. 1c and 1d), the rms roughness decreased from 27.7 to 6.04 nm when the growth temperature was increased from 500 °C to 550 °C. The cross-sectional scanning electron microscopy (SEM) image (Fig. 2a) of sample S2 shows that about a 200 nm thick Ga_2O_3 film was obtained from the 500 °C growth on sapphire; however, a number of pits were also observable on the plan view SEM image in Fig. 2b. The plan view SEM images of samples S3 and S4 (Fig. 3a and 3b, respectively) demonstrate that the increase in growth temperature also resulted in larger Ga_2O_3 grain size for sample S4. We show later in this paper via TEM that the grains in sample S3 were polycrystalline, whereas the ones in sample S4 were indeed amorphous.

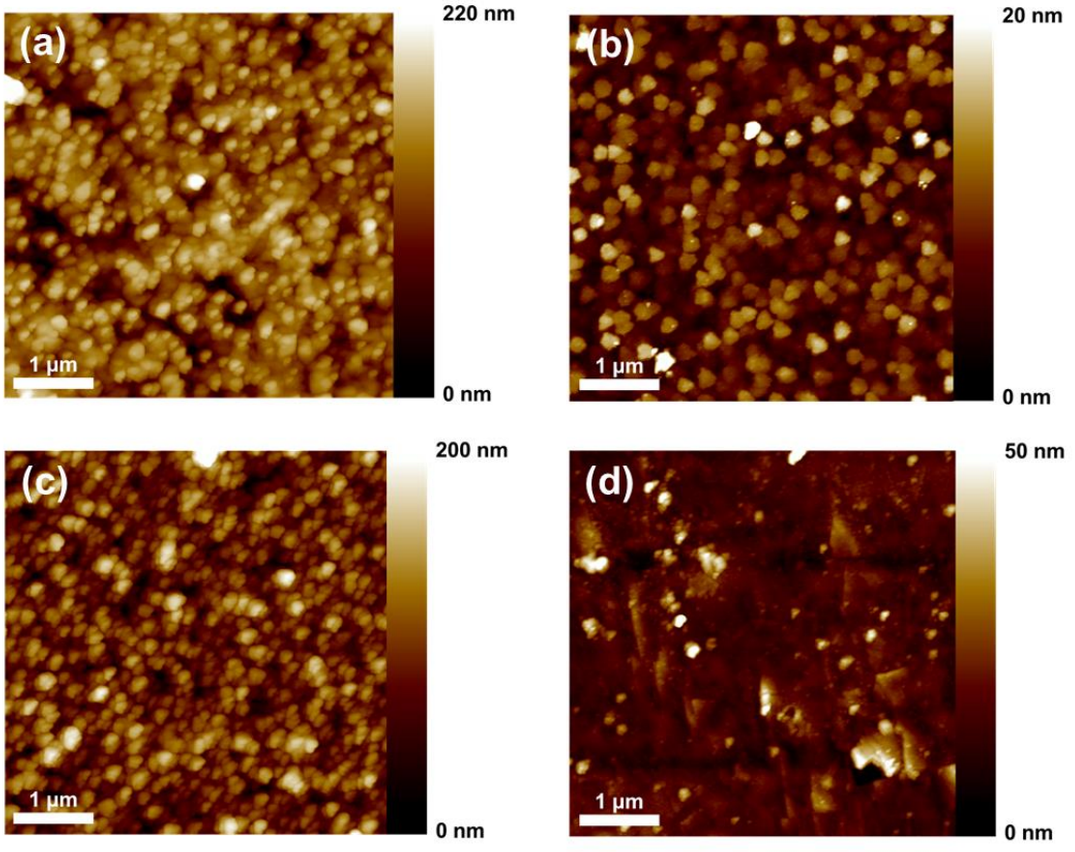

Figure 1. AFM images of HVPE α-Ga_2O_3 grown on c-Al_2O_3 substrates at (a) 450 °C (S1) and (b) 500 °C (S2) and nc-Ga_2O_3 grown on diamond at (c) 500 °C (S3) and (d) 550 °C (S4).

ACCEPTED MANUSCRIPT

Journal of Vacuum Science & Technology A

This is the author's peer reviewed, accepted manuscript. However, the online version of record will be different from this version once it has been copyedited and typeset.
PLEASE CITE THIS ARTICLE AS DOI: 10.1116/6.0002115

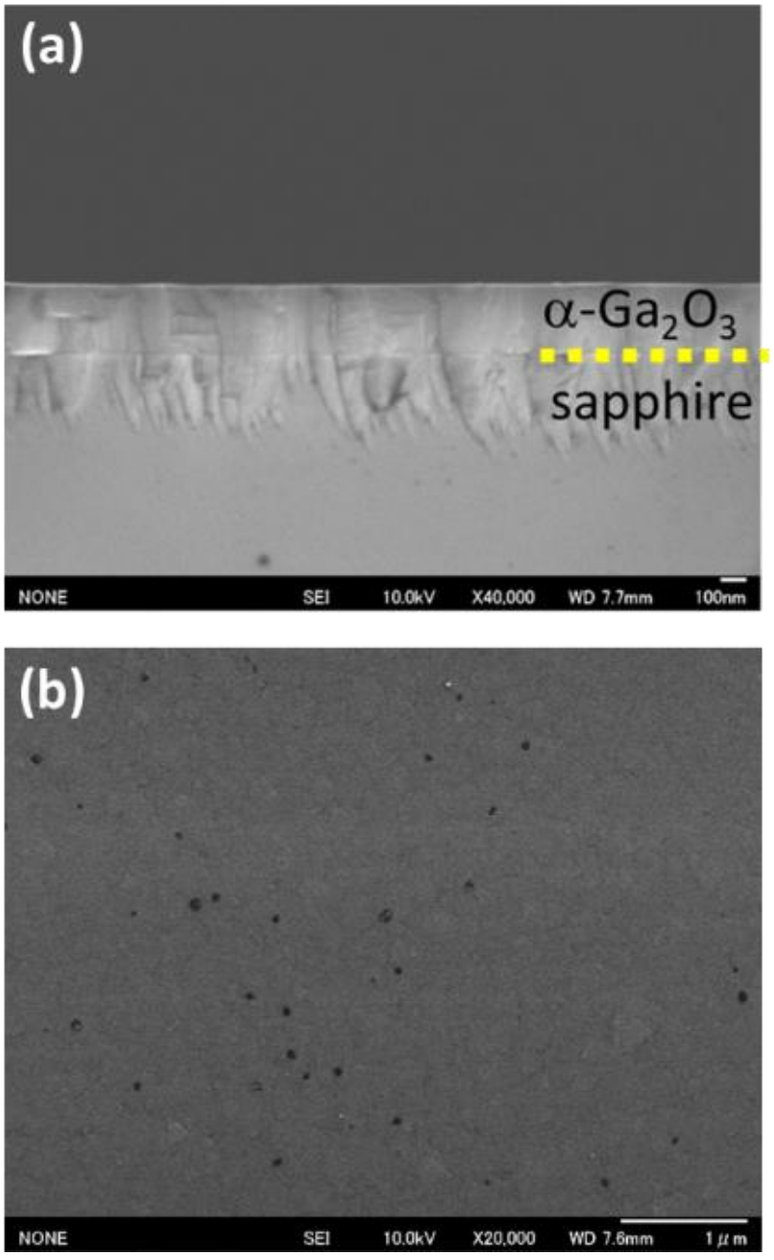

Figure 2. (a) Cross-sectional and (b) plan view scanning electron micrographs of HVPE α-Ga_2O_3 grown on c-Al_2O_3 substrates at 500 °C.

ACCEPTED MANUSCRIPT

Journal of Vacuum Science & Technology A

This is the author's peer reviewed, accepted manuscript. However, the online version of record will be different from this version once it has been copyedited and typeset.
PLEASE CITE THIS ARTICLE AS DOI: 10.1116/6.0002115

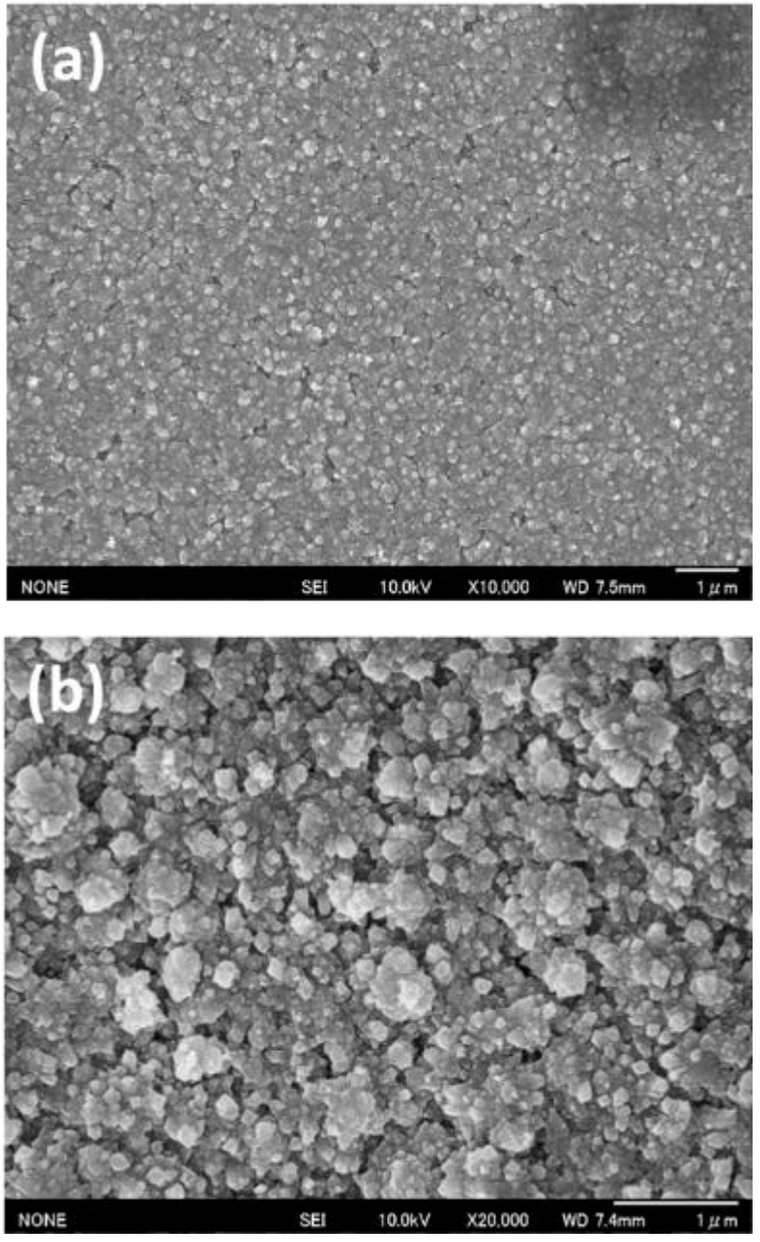

Figure 3. Plan view scanning electron micrographs of (a) sample S3 and (b) sample S4, showing HVPE growth of nc-Ga_2O_3 on diamond substrates.

The four samples of HVPE Ga_2O_3 films were examined via Raman spectroscopy next. The Raman spectrum of sample S2 shown in Fig. 4 confirmed that a corundum phase α-Ga_2O_3 film was obtained for 500 °C HVPE growth on sapphire. This was expected as the growth temperature was well below that required for the thermally-stable monoclinic phase. Somewhat surprisingly, the Raman spectra obtained across 10

ACCEPTED MANUSCRIPT
Journal of Vacuum Science & Technology A
This is the author's peer reviewed, accepted manuscript. However, the online version of record will be different from this version once it has been copyedited and typeset.
PLEASE CITE THIS ARTICLE AS DOI: 10.1116/6.0002115

locations on sample S3 (Fig. 5a) clearly indicate that monoclinic β-Ga_2O_3 was formed on the diamond substrate as a result of the 1 hour, 500 °C HVPE growth process. Similar Raman spectra indicating β-Ga_2O_3 formation were obtained from sample S4 as well (not shown here for brevity). Fig. 5b shows the same Raman spectra in the 1200-1800 cm^{-1} range showing strong diamond peaks at ~1330 cm^{-1} as well as the broad peaks around 1420 cm^{-1} attributed to the zero-phonon line of the nitrogen vacancy (N_V) center in diamond [28,29]. While Raman spectroscopy was not performed on these substrates prior to growth, we speculate that any existing N impurities in the diamond crystals could have been affected by the Ga_2O_3 growth process conditions, possibly contributing to the formation of N_V centers in the diamond substrates. In Fig. 5b, one Raman spectrum (location 5) exhibited peaks at ~1620 cm^{-1} and 1730 cm^{-1}, the origin of which is presently unknown. Fig. 6a shows an optical image of an approximately 20 μm × 20 μm area on sample S3 where a continuous monoclinic β-Ga_2O_3 film was observed. Fig. 6b shows a map of the β-Ga_2O_3 $A_g^{(3)}$ Raman mode (200 cm^{-1}) peak intensity from this area of sample S3. Outside of this location, the deposited Ga_2O_3 film did not exhibit monoclinic phase properties, likely due to diamond surface decomposition in oxygen environment during the initial stages of growth. Preventing diamond surface decomposition could be better achieved via a thin barrier layer in future growth experiments.

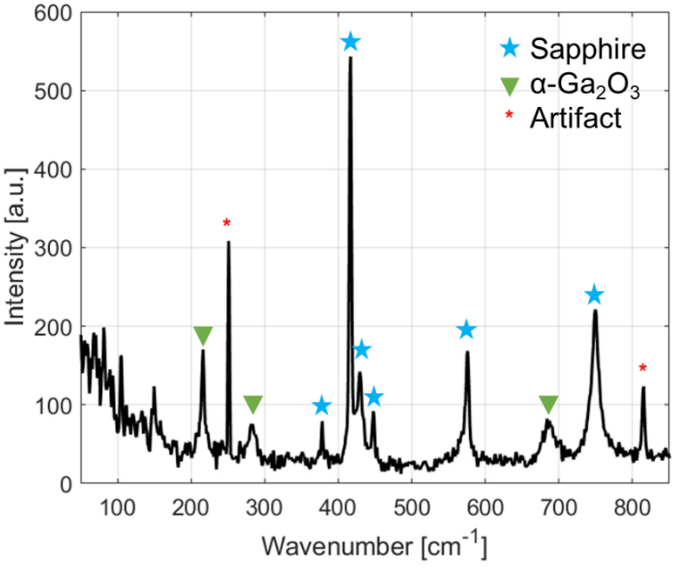

Figure 4. Raman spectrum from sample S2 (HVPE α-Ga_2O_3 on c-Al_2O_3). The peaks at ~250 cm^{-1} and 815 cm^{-1} were identified as artifacts originating from the instrument grating.

ACCEPTED MANUSCRIPT
Journal of Vacuum Science & Technology A
This is the author's peer reviewed, accepted manuscript. However, the online version of record will be different from this version once it has been copyedited and typeset.
PLEASE CITE THIS ARTICLE AS DOI: 10.1116/6.0002115

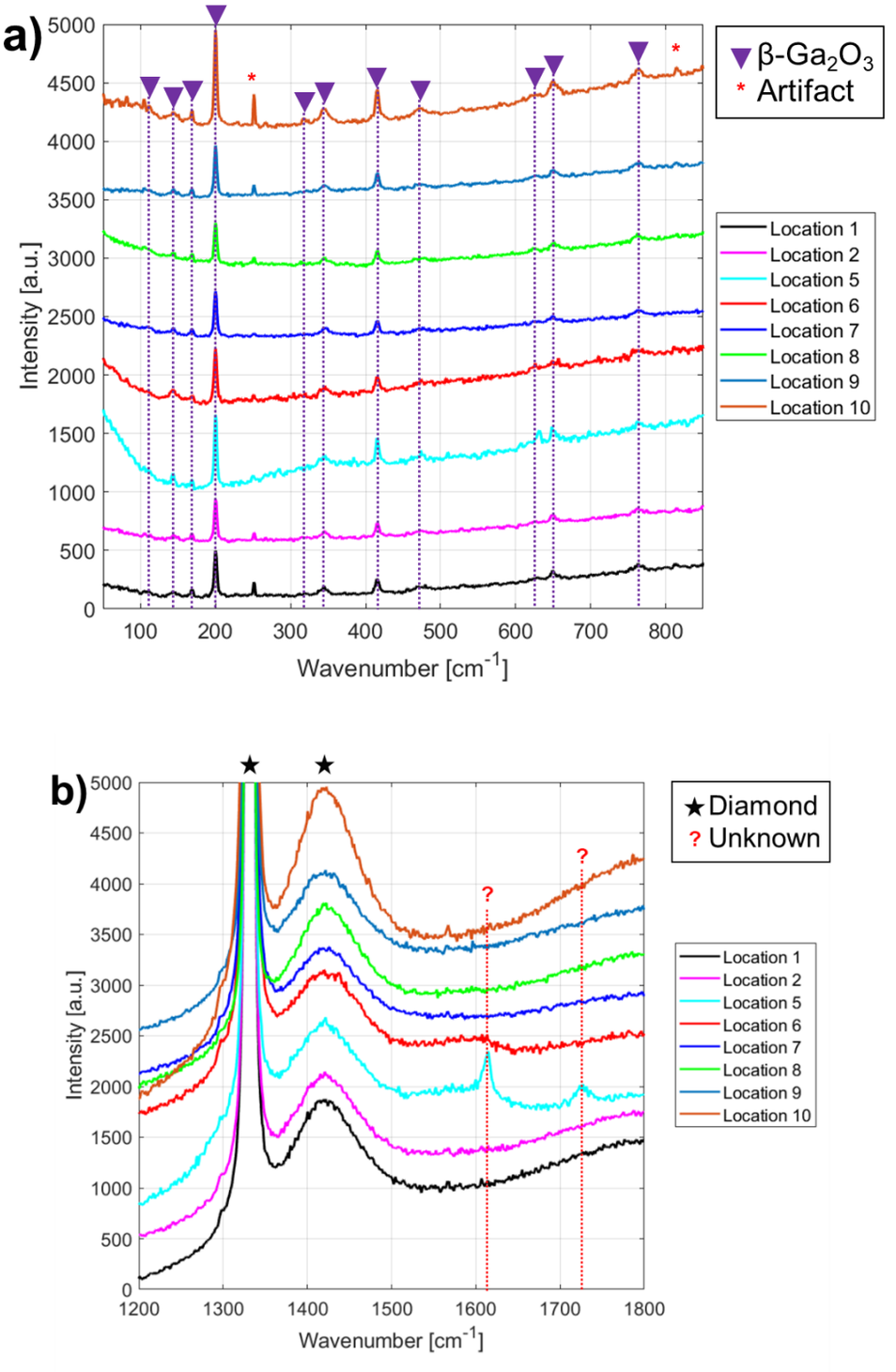

Figure 5. Raman spectra from sample S3 (HVPE Ga_2O_3 on diamond) in (a) the β-Ga_2O_3 spectral region (50-850 cm^{-1}) and (b) diamond spectral region (>1200 cm^{-1}). β-Ga_2O_3 peaks were clearly observed from multiple locations on the sample.

ACCEPTED MANUSCRIPT
Journal of Vacuum Science & Technology A
This is the author's peer reviewed, accepted manuscript. However, the online version of record will be different from this version once it has been copyedited and typeset.
PLEASE CITE THIS ARTICLE AS DOI: 10.1116/6.0002115

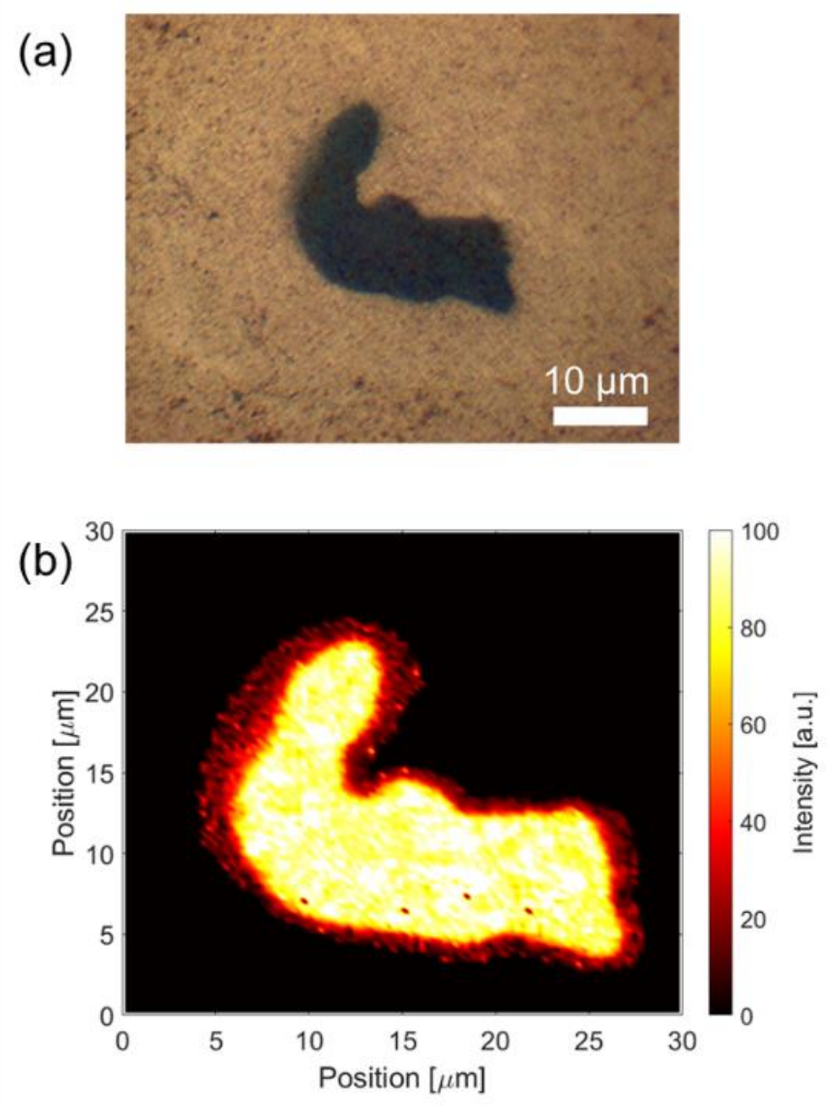

Figure 6. a) Optical image and b) map of the β-Ga_2O_3 $A_g^{(3)}$ Raman mode (200 cm^{-1}) peak intensity showing a β-Ga_2O_3 region on sample S3.

Figs. 7 and 8 show the XRD scans from the Ga_2O_3 films grown on sapphire and diamond substrates, respectively. The corundum α-Ga_2O_3 reflections were evident for the films on sapphire (Fig. 7), whereas no reflections from crystalline Ga_2O_3 were detected in Fig. 8. This result, while seemingly contrary to the prior discussion of the Raman data and the subsequent TEM images, was likely due to the very large probing volume of the X-ray diffractometer and the small volume of β-Ga_2O_3 regions compared to the nanocrystalline Ga_2O_3 surrounding them, resulting in very low signal-to-noise ratio in the XRD intensity.

ACCEPTED MANUSCRIPT
Journal of Vacuum Science & Technology A
This is the author's peer reviewed, accepted manuscript. However, the online version of record will be different from this version once it has been copyedited and typeset.
PLEASE CITE THIS ARTICLE AS DOI: 10.1116/6.0002115

While longer duration growths on diamond were not performed, we speculate that thicker Ga_2O_3 films on diamond can be obtained by this technique, similar to the result obtained recently via LPCVD [18].

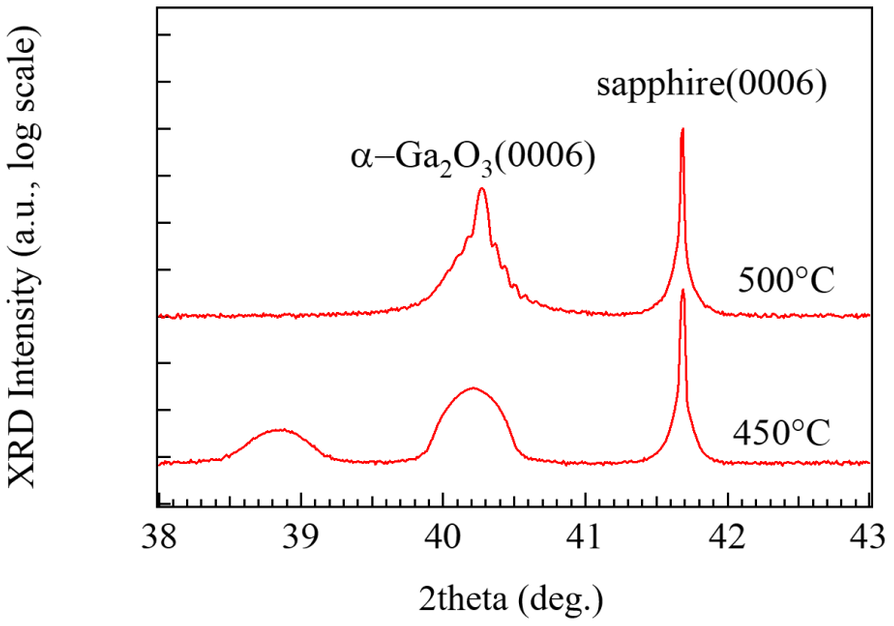

Figure 7. XRD scans of 450 °C (sample S1) and 500 °C (sample S2) HVPE α-Ga_2O_3 on c-Al_2O_3.

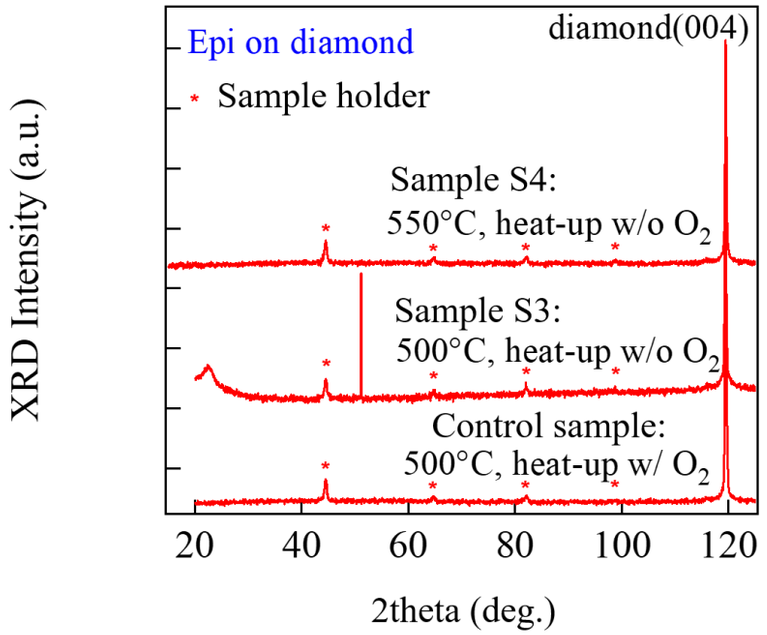

Figure 8. XRD scans of 500 °C (sample S3) and 550 °C (sample S4) HVPE nc-Ga_2O_3 on diamond.

ACCEPTED MANUSCRIPT
Journal of Vacuum Science & Technology A
This is the author's peer reviewed, accepted manuscript. However, the online version of record will be different from this version once it has been copyedited and typeset.
PLEASE CITE THIS ARTICLE AS DOI: 10.1116/6.0002115

The TEM images of cross-section of sample S1and S2 are shown in Figs. 9a-b and 9e-f, respectively. The thickness of sample S1 and S2 were found to be ~90 nm and ~140 nm, respectively. The nano-diffraction pattern of sample S1 (taken on the spot shown in inset of Fig. 9b) along $[1\bar{1}0]$ zone axis is presented in Fig. 9c. Sample S1 also exhibited a rhombohedral α-Ga_2O_3 crystal structure, as confirmed by the calculated d-spacing values of 0.226, 0.223, 0.258, and 0.458 nm corresponding to (113), $(11\bar{3})$, $(\bar{1}\bar{1}0)$, and (003) planes of α-Ga_2O_3, respectively. The nano-diffraction pattern of sample S2 (taken on the spot shown in inset of Fig. 9f) along the zone axis of $[\bar{1}\bar{1}0]$ is presented in Fig. 9g. The d-spacing values of the planes $(\bar{1}10)$, $(1\bar{1}\bar{4})$, $(1\bar{1}4)$, and (004) are calculated to be 0.454, 0.281, 0.256, and 0.331 nm, respectively, which confirms the rhombohedral crystal structure, i.e., α-Ga_2O_3 polymorph of the as-grown sample S2. The SAED patterns of both samples S1 and S2 demonstrate very good crystal quality of the overall film as evident in Figs. 9d and 9h, respectively.

The cross-sectional TEM images of sample S3 (MWE2) and sample S4 (MWE3) are shown in Figs. 10a-b and 10e-f, respectively. The thickness of samples S3 and S4 were found to be ~270 nm and ~60 nm, respectively. The nano-diffraction pattern of S3 (taken on the spot shown in insets of Fig. 10b) are presented in Fig. 10c. The calculated d-spacing values of (013), $(50\bar{1})$, $(5\bar{1}\bar{4})$, and $(\bar{5}\bar{1}\bar{2})$ planes along the zone axis of $[1\overline{15}5]$ are found to be 0.162, 0.242, 0.126, and 0.145 nm, respectively, which reveals the presence of monoclinic β-polymorph of Ga_2O_3. The SAED pattern, shown in Fig. 10d, of the overall S3 film indicated randomly oriented polycrystalline structure of Ga_2O_3. Figure 10g shows the nano-diffraction pattern of sample S4 along $[0\bar{1}0]$ zone axis. The d-spacing values of the planes $(10\bar{2})$, (401), $(\bar{5}01)$, and $(\bar{3}0\bar{3})$ are calculated to be 0.297, 0.254, 0.253, and 0.161 nm, respectively, demonstrating the presence of β-Ga_2O_3. The SAED pattern of sample S4, shown in Fig. 10h, reveals the amorphous nature of the film with randomly oriented nanocrystals of Ga_2O_3.

ACCEPTED MANUSCRIPT
Journal of Vacuum Science & Technology A
This is the author's peer reviewed, accepted manuscript. However, the online version of record will be different from this version once it has been copyedited and typeset.
PLEASE CITE THIS ARTICLE AS DOI: 10.1116/6.0002115

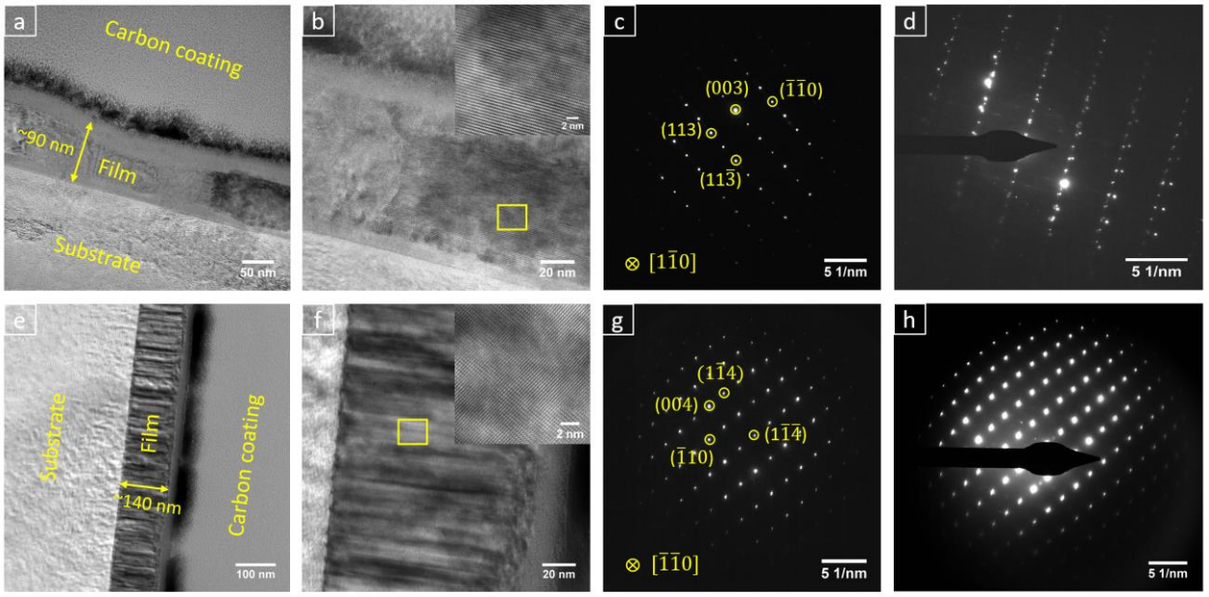

Figure 9. Cross-sectional bright field TEM images of (a-b) S1 (450 °C on sapphire) and (e-f) S2 (500 °C on sapphire); nano-diffraction patterns of (c) S1 along [1$\bar{1}$0] zone axis and (g) S2 along [$\bar{1}\bar{1}$0] zone axis; SAED patterns of (d) S1 and (h) S2.

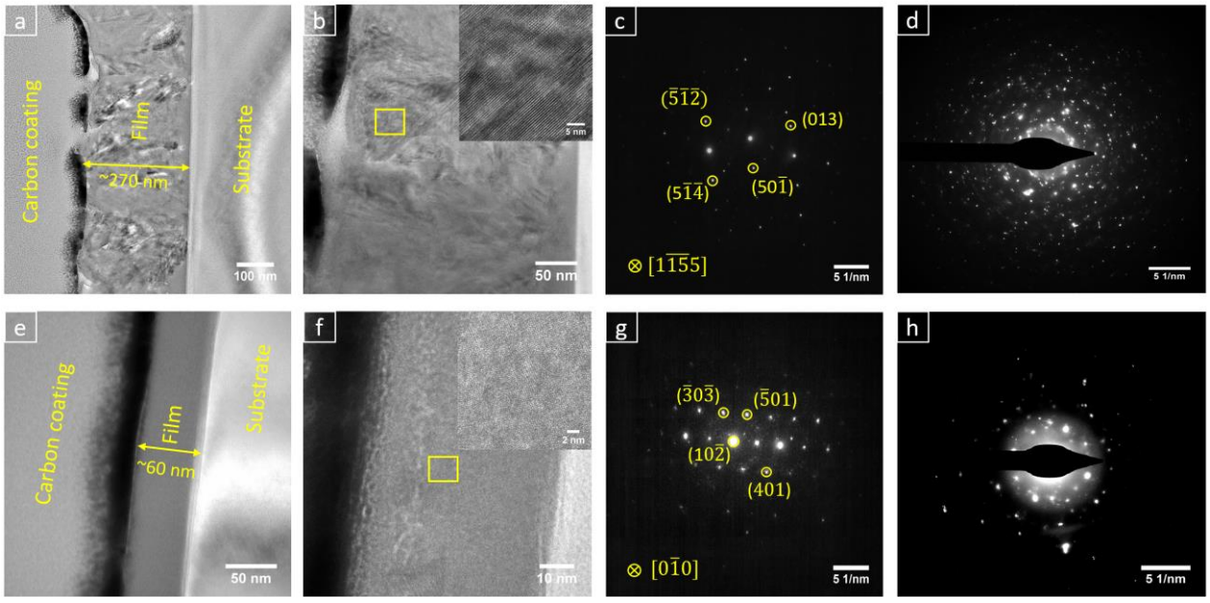

Figure 10. Cross-sectional bright field TEM images of (a-b) sample S3 (500 °C on diamond) and (e-f) sample S4 (550 °C on diamond); nano-diffraction patterns of (c) sample S3 along [1$\bar{1}\bar{5}$5] zone axis and (g) sample S4 along [0$\bar{1}$0] zone axis; SAED patterns of (d) sample S3 and (h) sample S4.

ACCEPTED MANUSCRIPT
Journal of Vacuum Science & Technology A
This is the author's peer reviewed, accepted manuscript. However, the online version of record will be different from this version once it has been copyedited and typeset.
PLEASE CITE THIS ARTICLE AS DOI: 10.1116/6.0002115

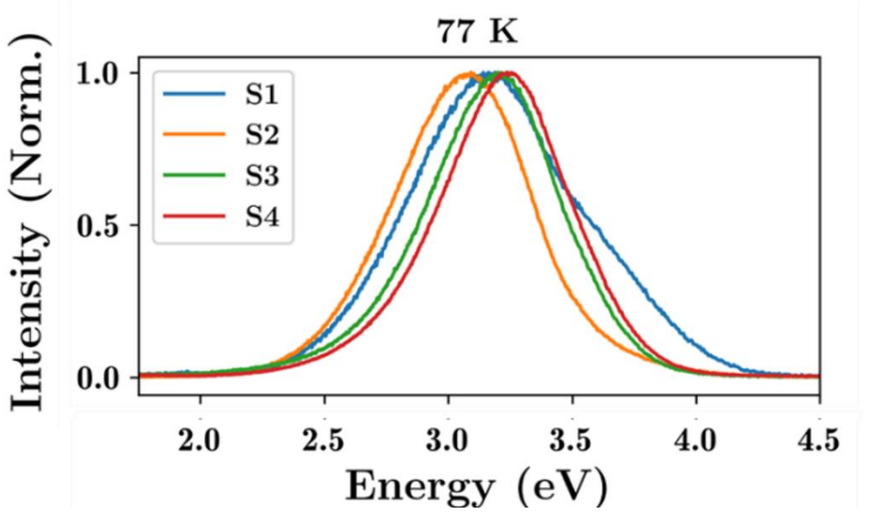

Figure 11. Cathodoluminescence emission spectra (normalized) for samples S1-S4 at 77 K.

Normalized CL emission from samples S1-S4 at 77 K is shown in Fig. 11 for comparison of peak location and relative shape of the spectrum. CL emission in samples S1-S4 is observed over similar range of energies that are typical for CL emission of β-Ga_2O_3. Gaussian decomposition (Fig. 12) of the CL emission shows the presence of three bands, UVL′, UVL, and BL, centered at approximately 3.7 eV, 3.2 eV, and 2.7 eV. The literature on luminescence in α-Ga_2O_3 is scarce: Moriya et al. have reported UVL' (3.7 eV) and BL (2.8 eV) emission in α-Ga_2O_3 grown on m-Al_2O_3 via mist-CVD, where the intensity of the latter was heavily dependent on the Sn concentration in the film [30]. Polyakov et al. have reported CL of α-Ga_2O_3 grown on c-Al_2O_3 and similarly to Moriya observed large dependence on doping density and the absence of band edge emission [31]. For the case of β-Ga_2O_3, observed here in samples S3 and S4 via Raman and TEM, the UVL′ and UVL bands are attributed to recombination of self-trapped excitons at O(I) and O(II) sites, with emission at 3.5-3.7 eV and 3.0-3.3 eV, respectively. In β-Ga_2O_3, UVL' and UVL bands pertain to the recombination of self-trapped excitons with large Stokes shift, which is also impurity independent [32-34]. BL is attributed to donor-acceptor pair recombination involving oxygen vacancy (V_O) donors and gallium vacancy (V_{Ga}) acceptors and their complexes [30,33]. Interestingly, the three primary luminescence bands of β-Ga_2O_3 are also observed in α-Ga_2O_3 within the same range of emission energy. UVL exhibited the highest

ACCEPTED MANUSCRIPT
Journal of Vacuum Science & Technology A
This is the author's peer reviewed, accepted manuscript. However, the online version of record will be different from this version once it has been copyedited and typeset.
PLEASE CITE THIS ARTICLE AS DOI: 10.1116/6.0002115

intensity of the three bands, followed by BL and UVL′. Contrary to the observation in samples S2-S4, the intensity of UVL′ was higher than that of BL in sample S1.

The temperature dependence of the luminescence intensity is shown in Fig. 13. Samples S1-S4 showed thermal quenching with increasing temperature. This is characteristic of thermal activation of additional recombination channels, which are non-radiative in nature. The activation energy associated with thermal quenching can be calculated with the following equation:

$$I(T) = I_0/(1 + Ae^{-E_A/k_BT}). \quad (1)$$

In Eqn. 1, I_0 is the integrated CL intensity at 0 K, A and E_A are the amplitude and thermal activation energy of the temperature activated processes, k_B is the Boltzmann constant, and T is the temperature. E_A for UVL′ , UVL, and BL are given in Table II.

Except for BL in sample S1, the activation energies for samples S1, S2, and S4 are comparable, suggesting a single recombination channel responsible for the thermal quenching of the CL emission intensity. There is a significant difference in E_A for the UVL′, UVL, and BL bands in sample S3, which indicates there are other contributing factors in addition to the activation of a non-radiative recombination channel.

The temperature-dependent shift of the UVL', UVL, and BL bands is presented in Fig. 14. Sample S1 exhibited blue shift in the UVL' band, red shift in the UVL band, and no significant shift in the BL band as a function of temperature. Sample S2 did not exhibit significant temperature dependent shift in the three constituent CL emission bands. Samples S3 and S4 both exhibited blue shift in the UVL' band and red shift in the UVL and BL bands. We note that temperature-dependent analysis of the Ga_2O_3 sub-bands has only been reported by Hidouri et al. for the hexagonal (ε) phase of Ga_2O_3.[35] Proper interpretation of the origin of the temperature-dependent energy shift of each CL emission sub-band requires further experimentation using phase-pure, homoepitaxial β-Ga_2O_3.

ACCEPTED MANUSCRIPT
Journal of Vacuum Science & Technology A
This is the author's peer reviewed, accepted manuscript. However, the online version of record will be different from this version once it has been copyedited and typeset.
PLEASE CITE THIS ARTICLE AS DOI: 10.1116/6.0002115

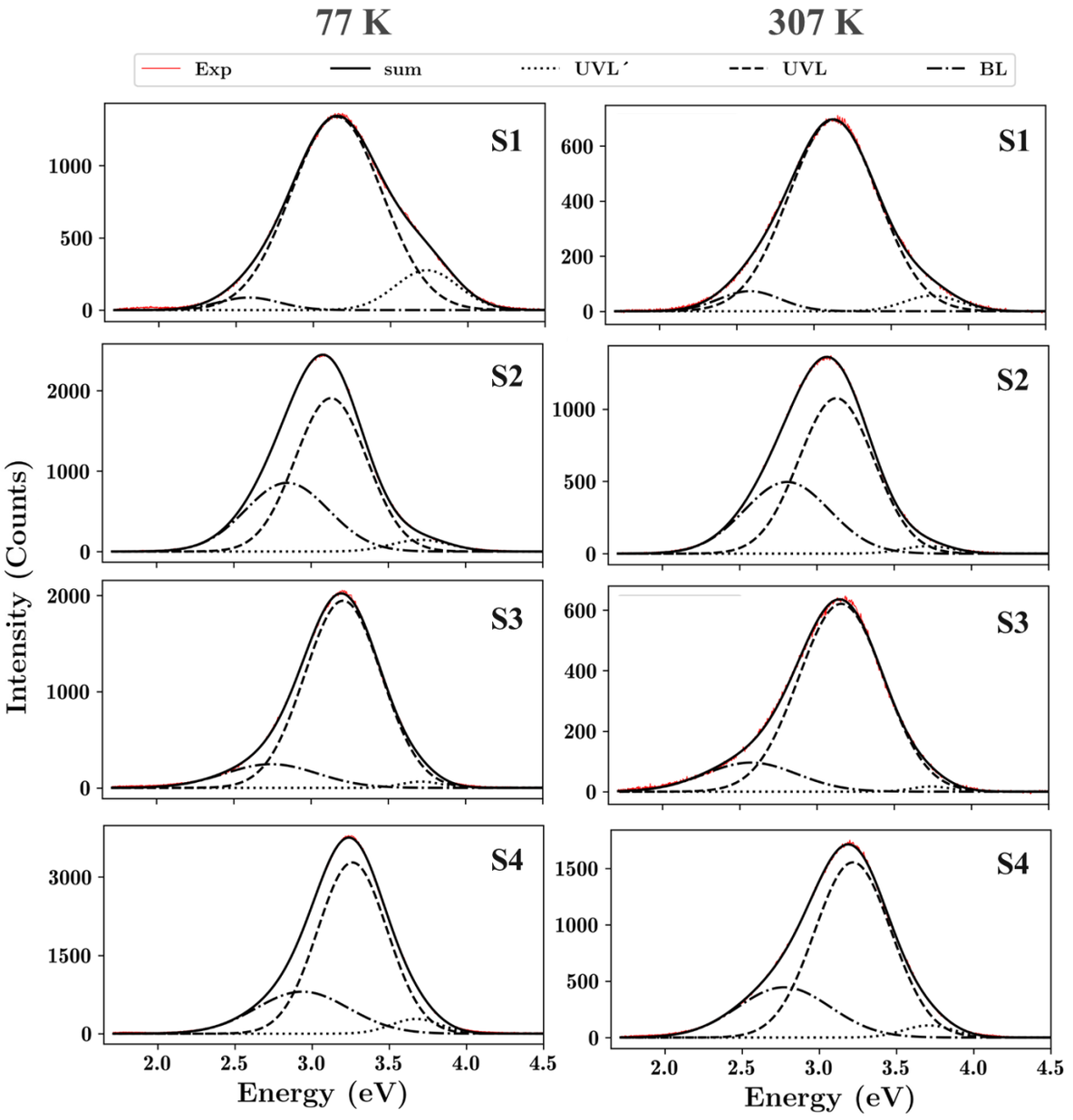

Figure 12. Gaussian decomposition of cathodoluminescence emission from samples S1-S4 (rows) at 77 K (left column) and 307 K (right column).

ACCEPTED MANUSCRIPT
Journal of Vacuum Science & Technology A
This is the author's peer reviewed, accepted manuscript. However, the online version of record will be different from this version once it has been copyedited and typeset.
PLEASE CITE THIS ARTICLE AS DOI: 10.1116/6.0002115

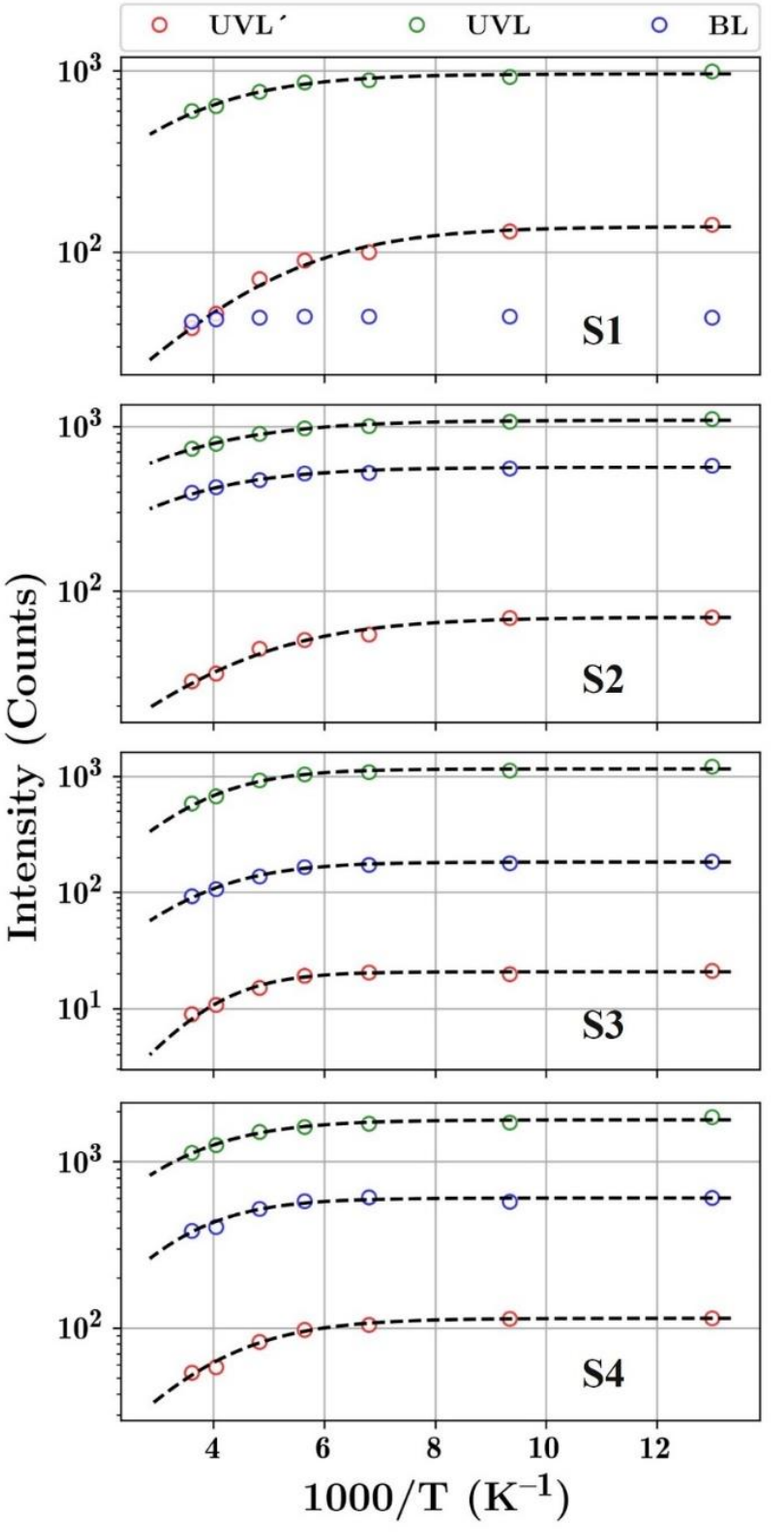

Figure 13. Temperature dependence of UVL′, UVL, and BL bands in samples S1-S4. Activation energy (Table II) is obtained by fitting the curves (dashed lines) with Eqn. (1).

ACCEPTED MANUSCRIPT
Journal of Vacuum Science & Technology A
This is the author's peer reviewed, accepted manuscript. However, the online version of record will be different from this version once it has been copyedited and typeset.
PLEASE CITE THIS ARTICLE AS DOI: 10.1116/6.0002115

Table II – Summary of activation energies measured via cathodoluminescence on samples S1-S4.

Sample	Activation Energy, E_A (meV)		
	UVL′	UVL	BL
S1	60.2	65.2	-
S2	58	57.5	62.3
S3	112.7	94.4	86.3
S4	76.8	76.5	89.4

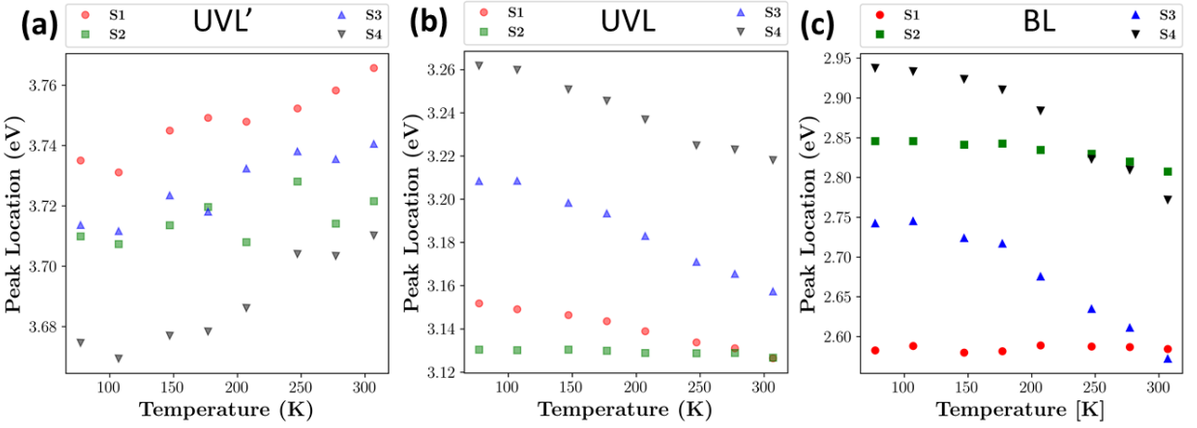

Figure 14. Temperature dependence of the peak location for (a) UVL', (b) UVL and (c) BL for samples S1-S4. UVL' and UVL from S1 exhibit weak blue and red shift, respectively. BL peak for this sample does not vary with temperature. UVL', UVL and BL for S2 show very little temperature dependence. UVL' exhibits blue shift and UVL/BL show red shift in S3/S4.

Conclusion

The experimental results presented in this study characterized the morphological and structural properties of HVPE Ga_2O_3 grown without a barrier dielectric on c-plane sapphire and diamond substrates. From a thermal perspective, barrier dielectrics present additional thermal boundary resistance; thus, the possibility of direct growth should be investigated for substrate-side thermal management of Ga_2O_3 devices. AFM and SEM imaging demonstrated that large grain size films were formed with a significant degree of rms

ACCEPTED MANUSCRIPT
Journal of Vacuum Science & Technology A
This is the author's peer reviewed, accepted manuscript. However, the online version of record will be different from this version once it has been copyedited and typeset.
PLEASE CITE THIS ARTICLE AS DOI: 10.1116/6.0002115

roughness regardless of the substrate used. The growths on sapphire substrates resulted in corundum α-Ga_2O_3 films as evidenced by XRD and Raman. While XRD did not reveal the presence of either α-Ga_2O_3 or β-Ga_2O_3 for HVPE growth on diamond, Raman spectroscopy did identify small regions of β-Ga_2O_3 across the samples grown at both 500 °C and 550 °C. This observed difference in Ga_2O_3 phase was in agreement with previous reports of Ga_2O_3 growth under non-thermal equilibrium conditions.[36] Scanning electron microscopy revealed that thin films did deposit on the diamond substrates, and transmission electron microscopy identified the polycrystalline nature of the Ga_2O_3 film on sample S3. For all samples, cathodoluminescence spectroscopy in the 77-307 K range revealed three emission bands, similar to those in β-Ga_2O_3, which are attributed to recombination of self-trapped excitons (UVL and UVL′) and donor-acceptor pair recombination assisted by Ga and O vacancies (BL) in these films.

Acknowledgements

Research at the Naval Research Laboratory was supported by the Office of Naval Research. J.S.L. gratefully acknowledges support by the National Research Council Research Associateship Programs. The research at UCF was supported in part by the National Science Foundation (NSF; ECCS Award Nos. 1802208 and 2127916) and in part by the US-Israel Binational Science Foundation (Award No. 2018010) and NATO (Award No. G5748). The work at UF and PSU was performed as part of the Interaction of Ionizing Radiation with Matter University Research Alliance (IIRM-URA), sponsored by the Department of the Defense's Defense Threat Reduction Agency (Award No. HDTRA1-20-2-0002, monitored by Jacob Calkins) and also sponsored by NSF (DMR Award No. 1856662, monitored by J.H. Edgar). A.H. also acknowledges support from NSF (ECCS Award No. 2015795).

Author Declarations

The authors have no conflicts to disclose.

ACCEPTED MANUSCRIPT

Journal of Vacuum Science & Technology A

This is the author's peer reviewed, accepted manuscript. However, the online version of record will be different from this version once it has been copyedited and typeset.
PLEASE CITE THIS ARTICLE AS DOI: 10.1116/6.0002115

Data Availability

The data that support the findings of this study are available from the corresponding author upon reasonable request.

ACCEPTED MANUSCRIPT
Journal of Vacuum Science & Technology A
This is the author's peer reviewed, accepted manuscript. However, the online version of record will be different from this version once it has been copyedited and typeset.
PLEASE CITE THIS ARTICLE AS DOI: 10.1116/6.0002115

References

[1] S.J. Pearton, J. Yang, P.H. Cary, F. Ren, J. Kim, M.J. Tadjer, and M.A. Mastro, Applied Physics Reviews **5**, 011301 (2018).

[2] M. Higashiwaki, K. Sasaki, A. Kuramata, T. Masui, and S. Yamakoshi, Applied Physics Letters **100**, 013504 (2012).

[3] M. Higashiwaki and S. Fujita, *Gallium Oxide: Materials Properties, Crystal Growth, and Devices* (Springer Nature, 2020).

[4] S. Pearton, F. Ren, and M. Mastro, *Gallium Oxide: Technology, Devices and Applications* (Elsevier, 2018).

[5] P. Dong, Pengfei Dong, Jincheng Zhang, Qinglong Yan, Zhihong Liu, Peijun Ma, Hong Zhou and Yue Hao "6 kV/3.4 mΩ·cm2 Vertical β-Ga2O3 Schottky Barrier Diode With BV2/Ron,sp Performance Exceeding 1-D Unipolar Limit of GaN and SiC," IEEE Electron Dev. Lett., 43, 765 (2022), doi: 10.1109/LED.2022.3160366.

[6] Jincheng Zhang, Pengfei Dong, Kui Dang, Yanni Zhang, Qinglong Yan, Hu Xiang, Jie Su, Zhihong Liu, Mengwei Si, Jiacheng Gao, Moufu Kong, Hong Zhou & Yue Hao, Ultra-wide bandgap semiconductor Ga_2O_3 power diodes. Nat Commun 13, 3900 (2022). https://doi.org/10.1038/s41467-022-31664-y

[7] A. Bhattacharyya, S. Sharma, F. Alema, P. Ranga, S. Roy, C. Peterson, G. Seryogin, A. Osinsky, U. Singisetti, and S. Krishnamoorthy, Applied Physics Express **15**, 061001 (2022).

[8] M.H. Wong, H. Murakami, Y. Kumagai, and M. Higashiwaki, IEEE Electron Device Letters **41**, 296 (2020).

[9] Z. Hu, K. Nomoto, W. Li, Z. Zhang, N. Tanen, Q.T. Thieu, K. Sasaki, A. Kuramata, T. Nakamura, D. Jena, and H.G. Xing, Applied Physics Letters **113**, 122103 (2018).

ACCEPTED MANUSCRIPT
Journal of Vacuum Science & Technology A
This is the author's peer reviewed, accepted manuscript. However, the online version of record will be different from this version once it has been copyedited and typeset.
PLEASE CITE THIS ARTICLE AS DOI: 10.1116/6.0002115

[10] J.B. Varley, J.R. Weber, A. Janotti, and C.G. de Walle, Applied Physics Letters **97**, 142106 (2010).

[11] J.B. Varley, A. Janotti, C. Franchini, and C.G. de Walle, Physical Review B **85**, 081109 (2012).

[12] Z. Guo, A. Verma, X. Wu, F. Sun, A. Hickman, T. Masui, A. Kuramata, M. Higashiwaki, D. Jena, and T. Luo, Applied Physics Letters **106**, 111909 (2015).

[13] J.S. Lundh, H.N. Masten, K. Sasaki, A.G. Jacobs, Z. Cheng, J. Spencer, L. Chen, J. Gallagher, A.D. Koehler, K. Konishi, A. Kuramata, K.D. Hobart, and M.J. Tadjer, in *Device Research Conference - Conference Digest, DRC* (IEEE, 2022).

[14] Z. Cheng, L. Yates, J. Shi, M.J. Tadjer, K.D. Hobart, and S. Graham, APL Materials **7**, 031118 (2019).

[15] T. Matsumae, Y. Kurashima, H. Umezawa, K. Tanaka, T. Ito, H. Watanabe, and H. Takagi, Applied Physics Letters **116**, 141602 (2020).

[16] Y. Xu, F. Mu, Y. Wang, D. Chen, X. Ou, and T. Suga, Ceramics International **45**, 6552 (2019).

[17] M. Malakoutian, Y. Song, C. Yuan, C. Ren, J.S. Lundh, R.M. Lavelle, J.E. Brown, D.W. Snyder, S. Graham, S. Choi, and S. Chowdhury, Applied Physics Express **14**, 055502 (2021).

[18] M.R. Karim, Z. Chen, Z. Feng, H.-L. Huang, J.M. Johnson, M.J. Tadjer, J. Hwang, and H. Zhao, Journal of Vacuum Science & Technology A: Vacuum, Surfaces, and Films **39**, 023411 (2021).

[19] Z. Cheng, V.D. Wheeler, T. Bai, J. Shi, M.J. Tadjer, T. Feygelson, K.D. Hobart, M.S. Goorsky, and S. Graham, Applied Physics Letters **116**, 062105 (2020).

[20] A.Y. Polyakov, V.I. Nikolaev, S.A. Tarelkin, A.I. Pechnikov, S.I. Stepanov, A.E. Nikolaev, I. v. Shchemerov, E.B. Yakimov, N. v. Luparev, M.S. Kuznetsov, A.A. Vasilev, A.I. Kochkova, M.I. Voronova, M.P. Scheglov, J. Kim, and S.J. Pearton, Journal of Applied Physics **129**, 185701 (2021).

[21] C.H. Lin, N. Hatta, K. Konishi, S. Watanabe, A. Kuramata, K. Yagi, and M. Higashiwaki, Applied Physics Letters **114**, 032103 (2019).

ACCEPTED MANUSCRIPT
Journal of Vacuum Science & Technology A
This is the author's peer reviewed, accepted manuscript. However, the online version of record will be different from this version once it has been copyedited and typeset.
PLEASE CITE THIS ARTICLE AS DOI: 10.1116/6.0002115

[22] Y. Song, D. Shoemaker, J.H. Leach, C. McGray, H.-L. Huang, A. Bhattacharyya, Y. Zhang, C.U. Gonzalez-Valle, T. Hess, S. Zhukovsky, K. Ferri, R.M. Lavelle, C. Perez, D.W. Snyder, J.-P. Maria, B. Ramos-Alvarado, X. Wang, S. Krishnamoorthy, J. Hwang, B.M. Foley, and S. Choi, ACS Applied Materials & Interfaces **13**, 40817 (2021).

[23] Z. Cheng, F. Mu, T. You, W. Xu, J. Shi, M.E. Liao, Y. Wang, K. Huynh, T. Suga, M.S. Goorsky, X. Ou, and S. Graham, ACS Applied Materials and Interfaces **12**, 44943 (2020).

[24] T. Matsumae, Y. Kurashima, H. Takagi, H. Umezawa, and E. Higurashi, Journal of Applied Physics **130**, 085303 (2021).

[25] W. Xu, T. You, F. Mu, Z. Shen, J. Lin, K. Huang, M. Zhou, A. Yi, Z. Qu, T. Suga, G. Han, and X. Ou, ACS Applied Electronic Materials **4**, 494 (2021).

[26] D. Ma, G. Zhang, and L. Zhang, Journal of Physics D: Applied Physics **53**, 434001 (2020).

[27] M.E. Liao, C. Li, H.M. Yu, E. Rosker, M.J. Tadjer, K.D. Hobart, and M.S. Goorsky, APL Materials **7**, 022517 (2018).

[28] Y.N. Palyanov, I.N. Kupriyanov, and Y.M. Borzdov, Carbon N Y **143**, 769 (2019).

[29] M. Yang, Q. Yuan, J. Gao, S. Shu, F. Chen, H. Sun, K. Nishimura, S. Wang, J. Yi, C.-T. Lin, and N. Jiang, Nanomaterials **9**, (2019).

[30] R. Moriya, J. Kikawa, S. Mouri, T. Shinohe, S. Xiao, H. Miyake, T. Araki, Phys. Stat. Solidi B 259, 2100598 (2022).

[31] A. Polyakov, N.B. Smirnov, I.V. Shchemerov, E.B. Yakimov, V.I. Nikolaev, S.I. Stepanov, A.I. Pechnikov, A.V. Chernykh, K.D. Shcherbachev, A.S. Shikoh, A. Kochkova, A.A. Vasilev, S.J. Pearton, APL Mater. 7, 051103 (2019).

ACCEPTED MANUSCRIPT
Journal of Vacuum Science & Technology A
This is the author's peer reviewed, accepted manuscript. However, the online version of record will be different from this version once it has been copyedited and typeset.
PLEASE CITE THIS ARTICLE AS DOI: 10.1116/6.0002115

[32] Yamaga, M., T. Ishikawa, M. Yoshida, T. Hasegawa, E.G. Villora, and K. Shimamura, Polarization of optical spectra in transparent conductive oxide β-Ga2O3. physica status solidi (c), 8(9), 2621-2624 (2011).

[33] Shimamura, K., E.G. Víllora, T. Ujiie, and K. Aoki, Excitation and photoluminescence of pure and Si-doped β-Ga2O3 single crystals. Applied Physics Letters, 92(20), 201914 (2008).

[34] T. Harwig, F. Kellendonk, S. Slappendel, The ultraviolet luminescence of β-galliumsesquioxide, J. Phys. and Chem. of Solids 39 (6), 675-680 (1978).

[35] T. Hidouri, A. Parisini, S. Dadgostar, J. Jimenez, R. Fornari, Point defect localization and cathodoluminescence emission in undoped ε-Ga_2O_3, J. Phys. D: Appl. Phys. 55 295103 (2022).

[36] Ken Goto, Hidetoshi Nakahata, Hisashi Murakami, and Yoshinao Kumagai , "Temperature dependence of Ga_2O_3 growth by halide vapor phase epitaxy on sapphire and β-Ga_2O_3 substrates", Appl. Phys. Lett. 117, 222101 (2020) https://doi.org/10.1063/5.0031267.

ACCEPTED MANUSCRIPT

Journal of Vacuum Science & Technology A

This is the author's peer reviewed, accepted manuscript. However, the online version of record will be different from this version once it has been copyedited and typeset.
PLEASE CITE THIS ARTICLE AS DOI: 10.1116/6.0002115

ACCEPTED MANUSCRIPT

Journal of Vacuum
Science & Technology A

This is the author's peer reviewed, accepted manuscript. However, the online version of record will be different from this version once it has been copyedited and typeset.
PLEASE CITE THIS ARTICLE AS DOI: 10.1116/6.0002115

Journal of Vacuum Science & Technology A

ACCEPTED MANUSCRIPT

This is the author's peer reviewed, accepted manuscript. However, the online version of record will be different from this version once it has been copyedited and typeset.
PLEASE CITE THIS ARTICLE AS DOI: 10.1116/6.0002115

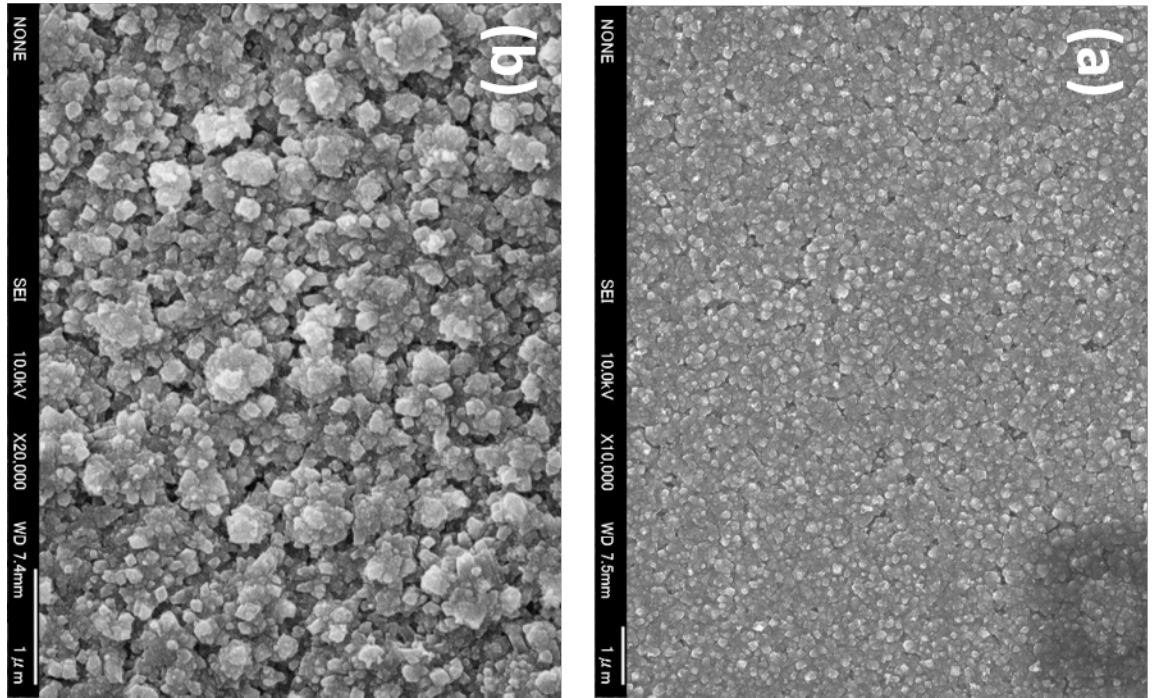

ACCEPTED MANUSCRIPT

Journal of Vacuum Science & Technology A

This is the author's peer reviewed, accepted manuscript. However, the online version of record will be different from this version once it has been copyedited and typeset.
PLEASE CITE THIS ARTICLE AS DOI: 10.1116/6.0002115

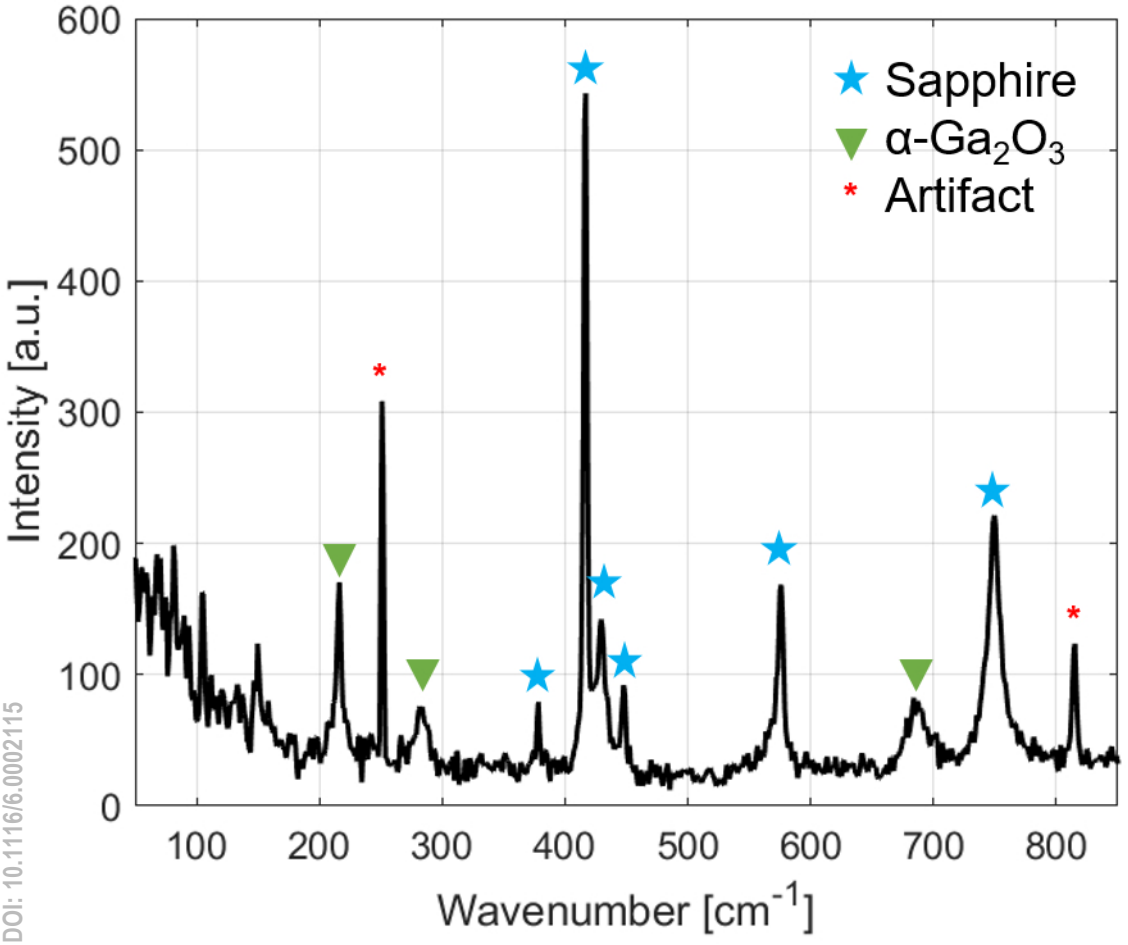

ACCEPTED MANUSCRIPT
Journal of Vacuum Science & Technology A
This is the author's peer reviewed, accepted manuscript. However, the online version of record will be different from this version once it has been copyedited and typeset.
PLEASE CITE THIS ARTICLE AS DOI: 10.1116/6.0002115

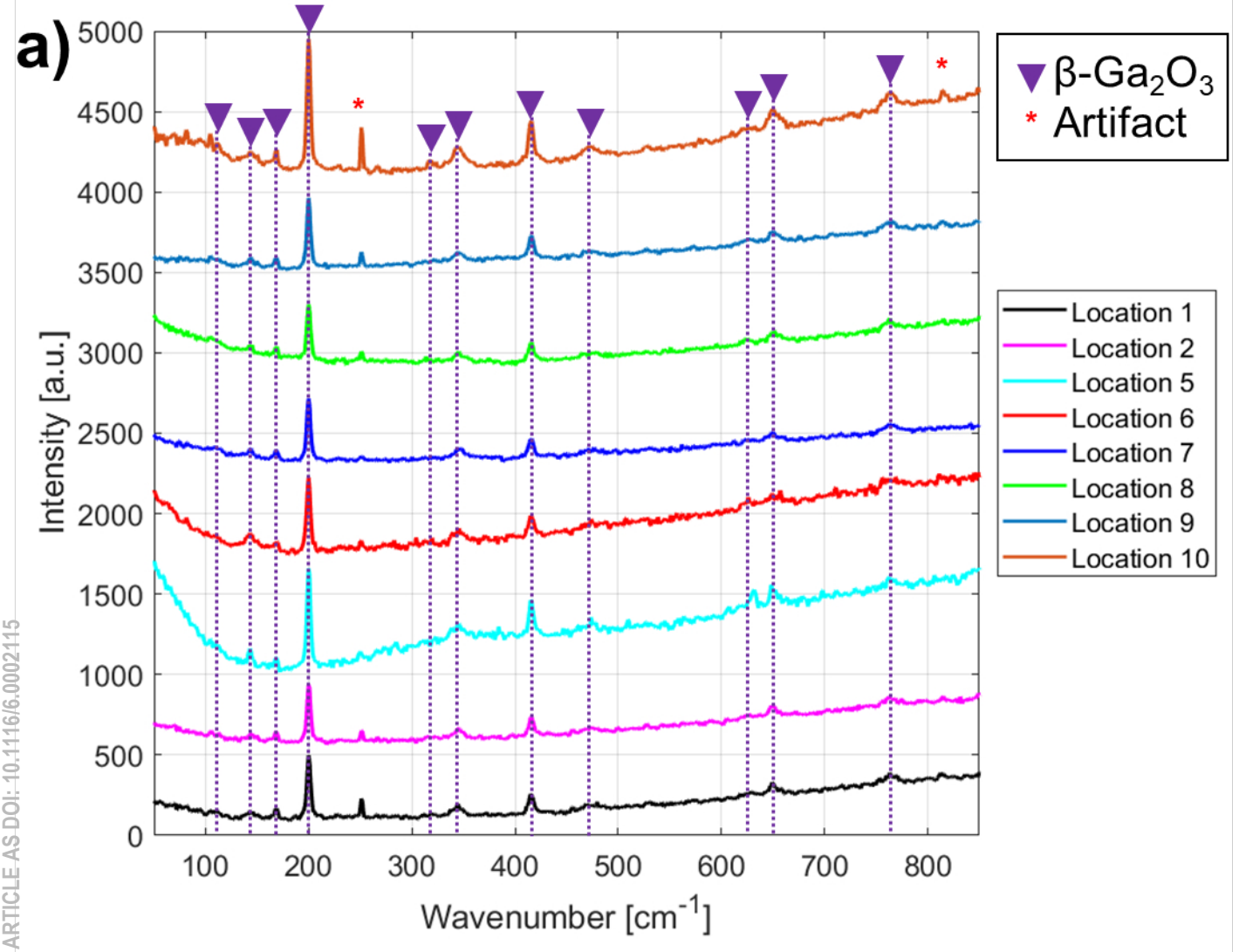

Journal of Vacuum Science & Technology A

ACCEPTED MANUSCRIPT

This is the author's peer reviewed, accepted manuscript. However, the online version of record will be different from this version once it has been copyedited and typeset.

PLEASE CITE THIS ARTICLE AS DOI: 10.1116/6.0002115

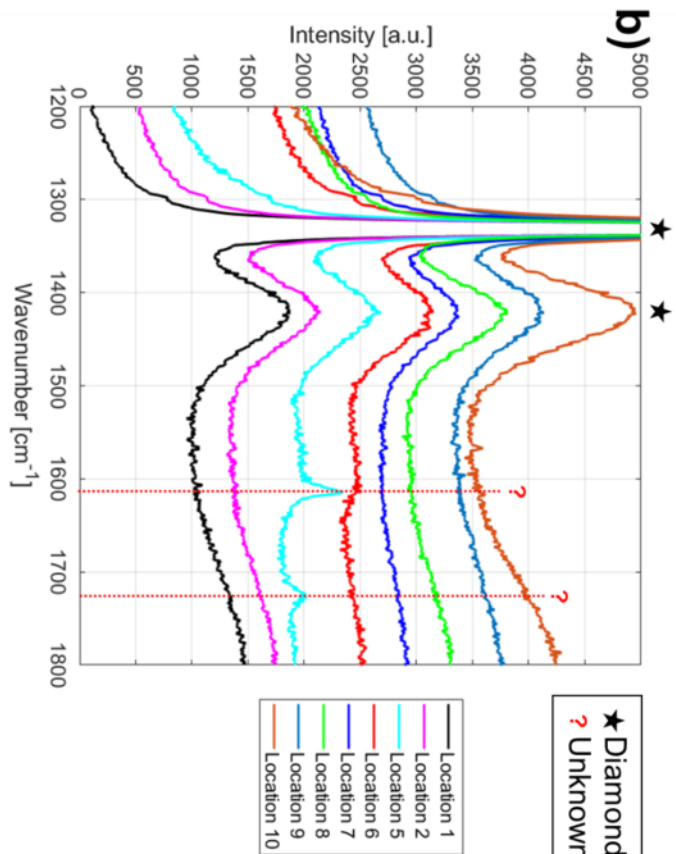

Journal of Vacuum Science & Technology A

ACCEPTED MANUSCRIPT

This is the author's peer reviewed, accepted manuscript. However, the online version of record will be different from this version once it has been copyedited and typeset.

PLEASE CITE THIS ARTICLE AS DOI: 10.1116/6.0002115

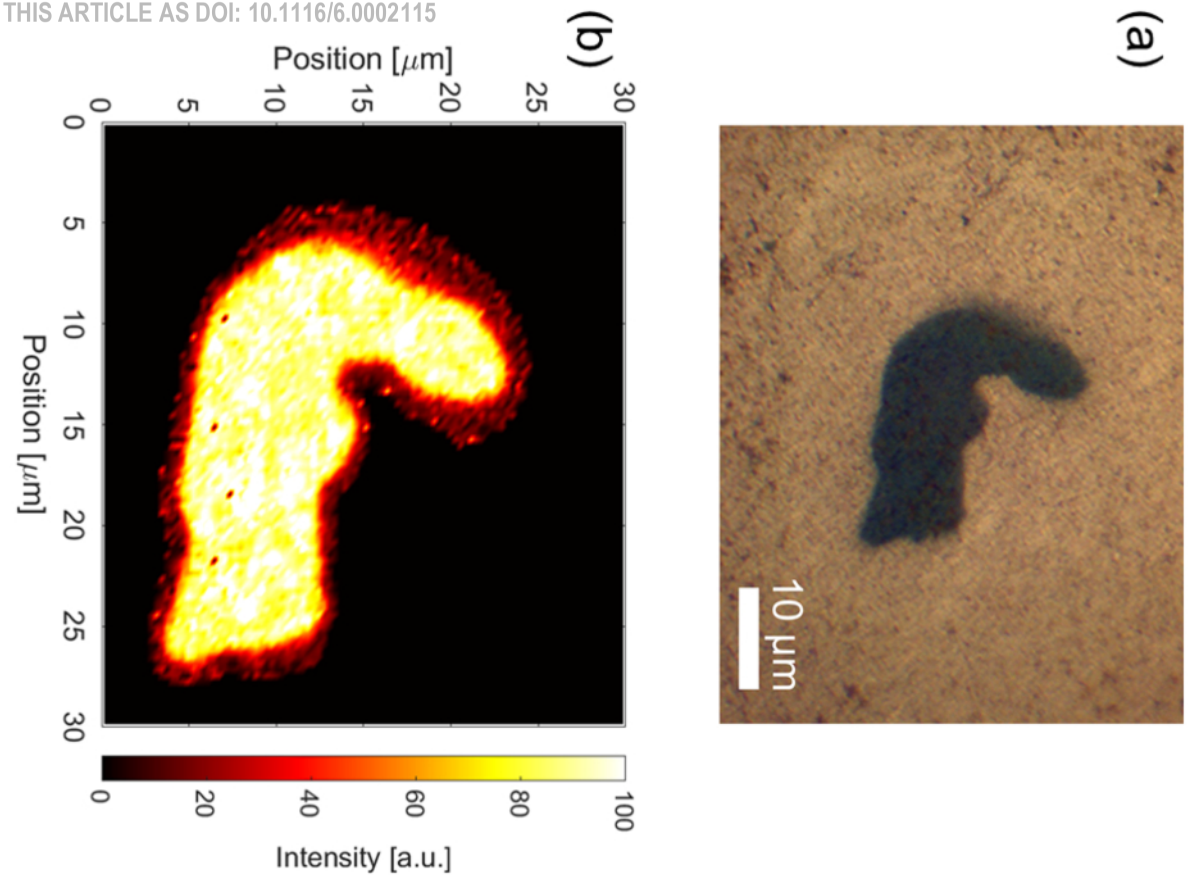

ACCEPTED MANUSCRIPT

Journal of Vacuum Science & Technology A

This is the author's peer reviewed, accepted manuscript. However, the online version of record will be different from this version once it has been copyedited and typeset.
PLEASE CITE THIS ARTICLE AS DOI: 10.1116/6.0001115

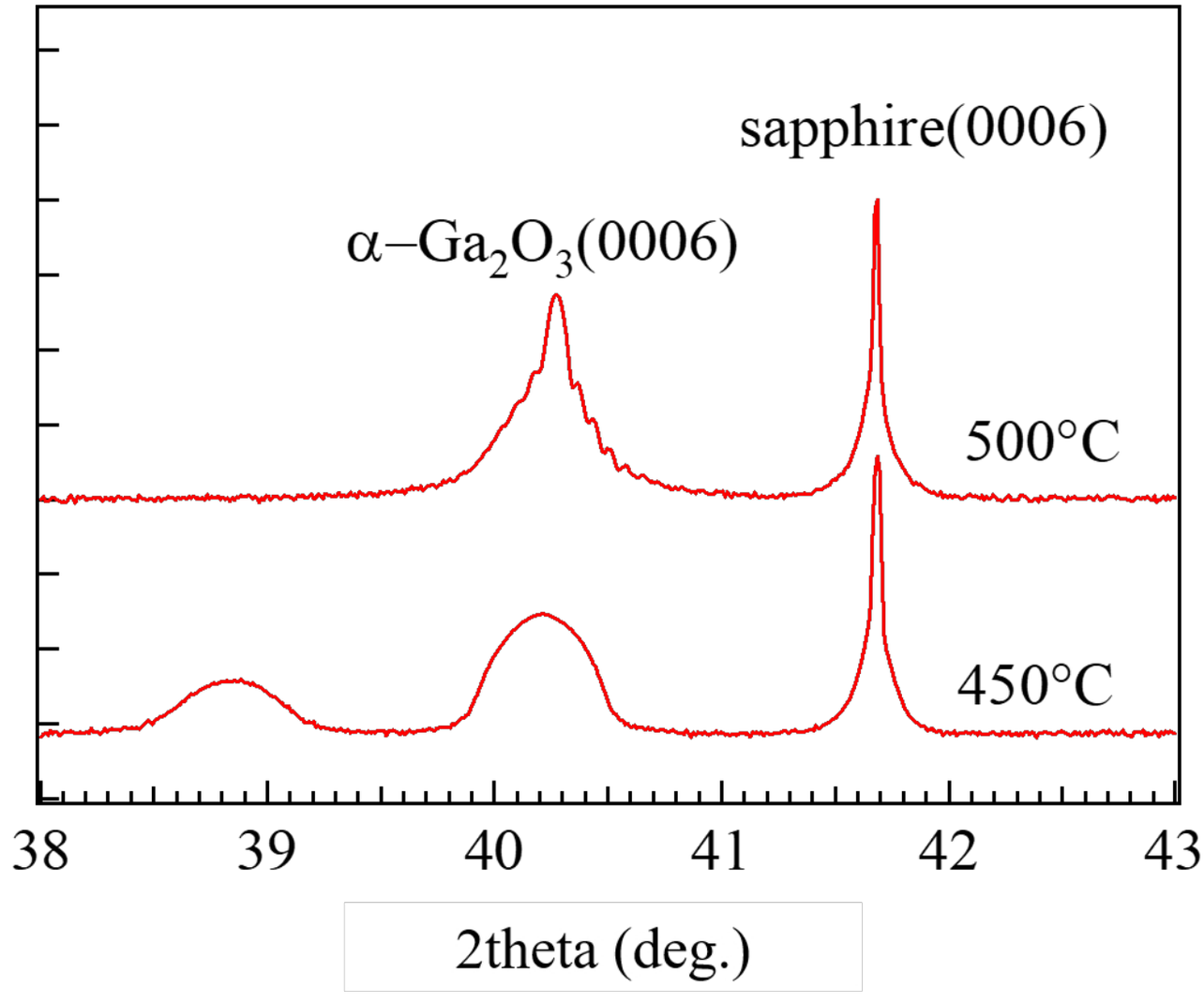

ACCEPTED MANUSCRIPT
Journal of Vacuum Science & Technology A
This is the author's peer reviewed, accepted manuscript. However, the online version of record will be different from this version once it has been copyedited and typeset.
PLEASE CITE THIS ARTICLE AS DOI: 10.1116/6.0002121

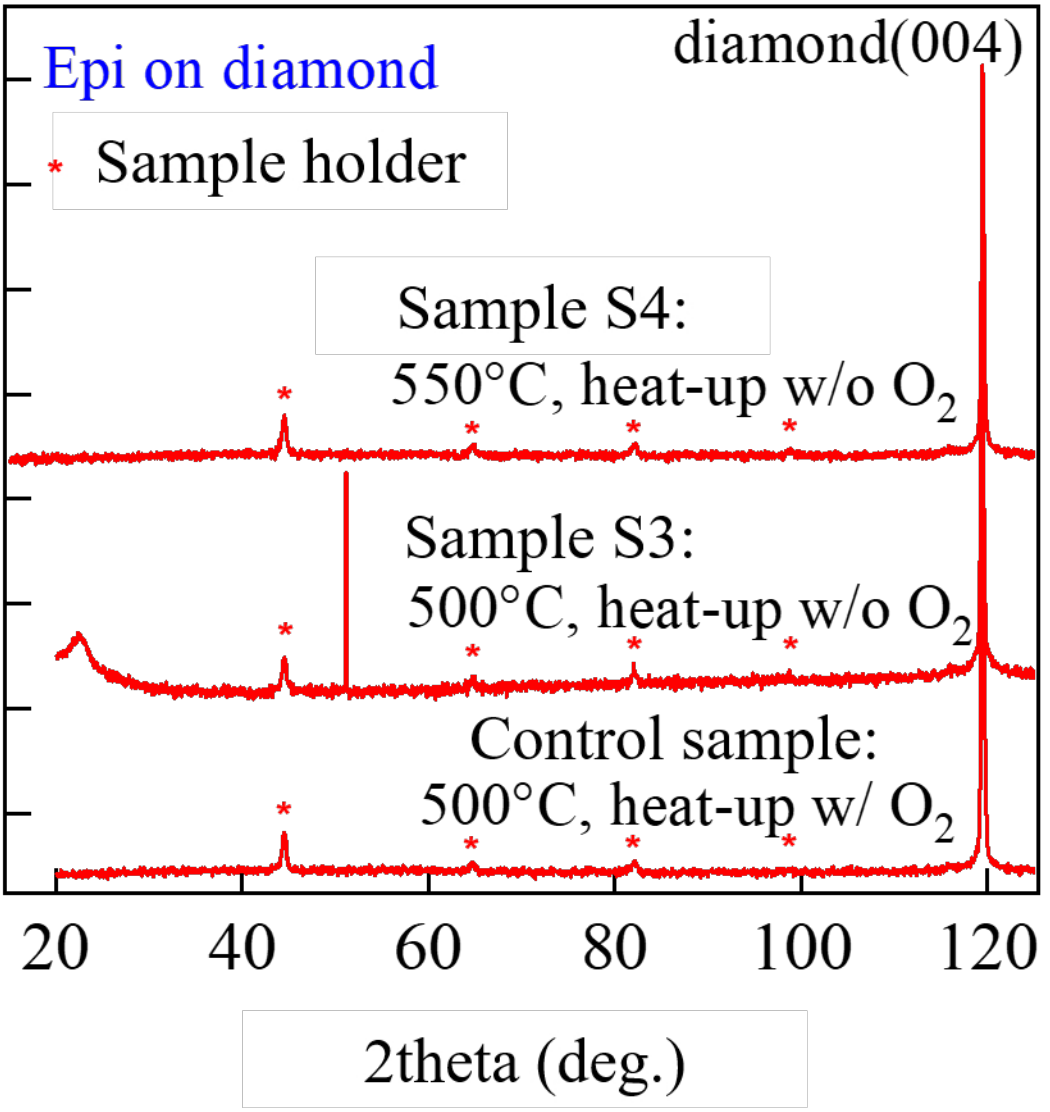

ACCEPTED MANUSCRIPT

Journal of Vacuum Science & Technology A

This is the author's peer reviewed, accepted manuscript. However, the online version of record will be different from this version once it has been copyedited and typeset.
PLEASE CITE THIS ARTICLE AS DOI:

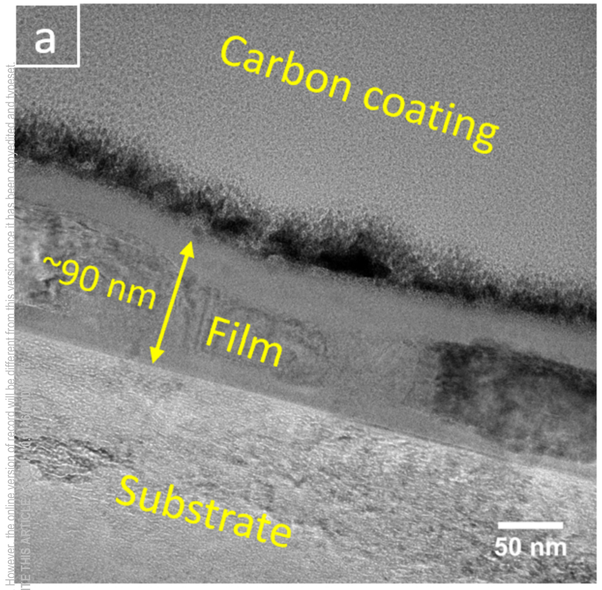

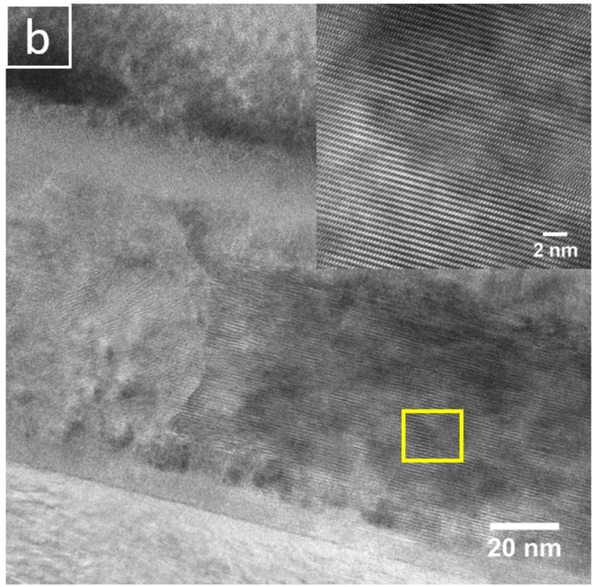

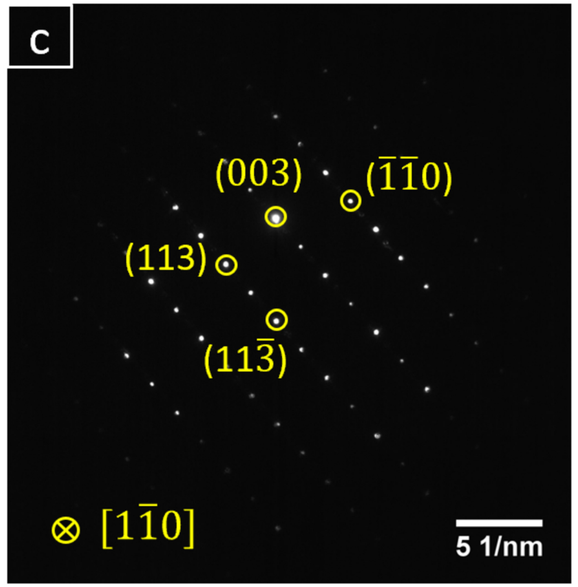

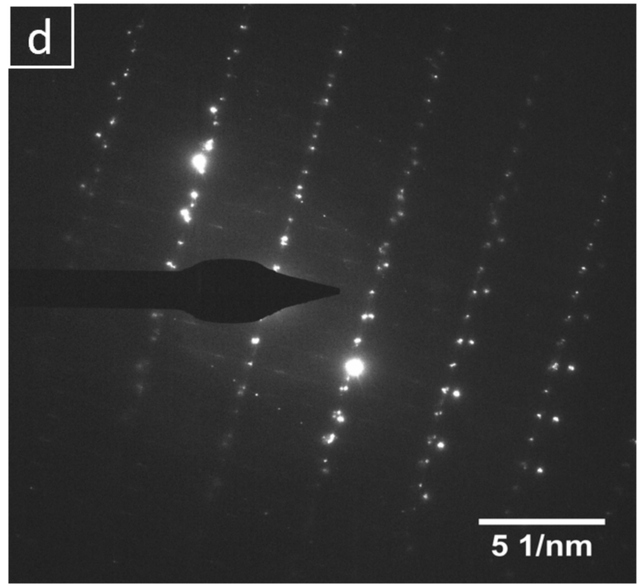

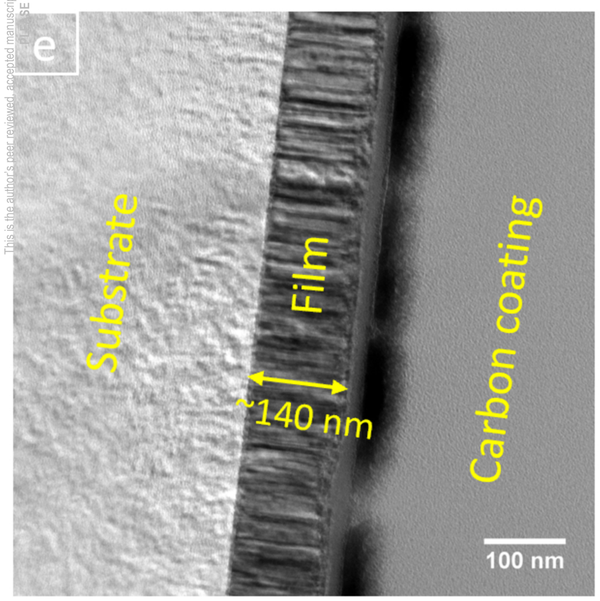

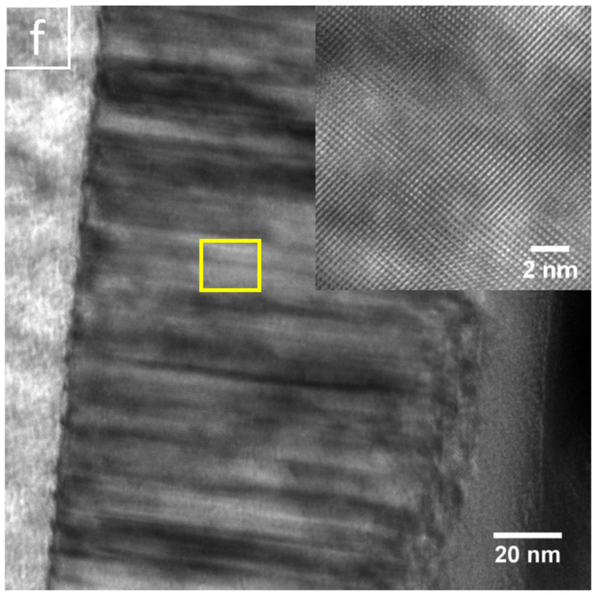

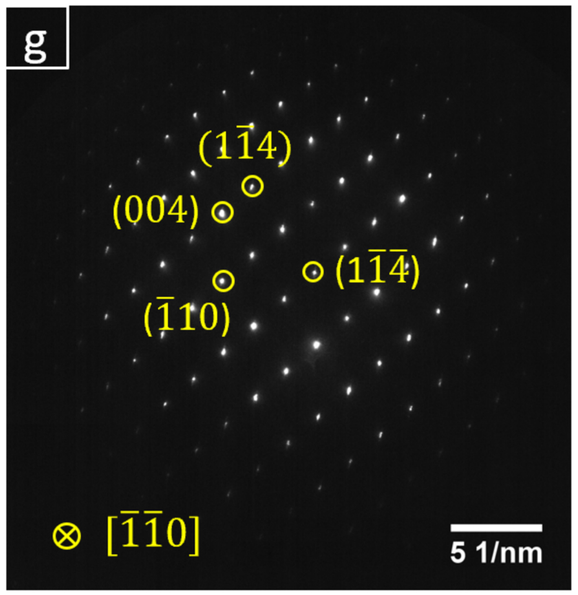

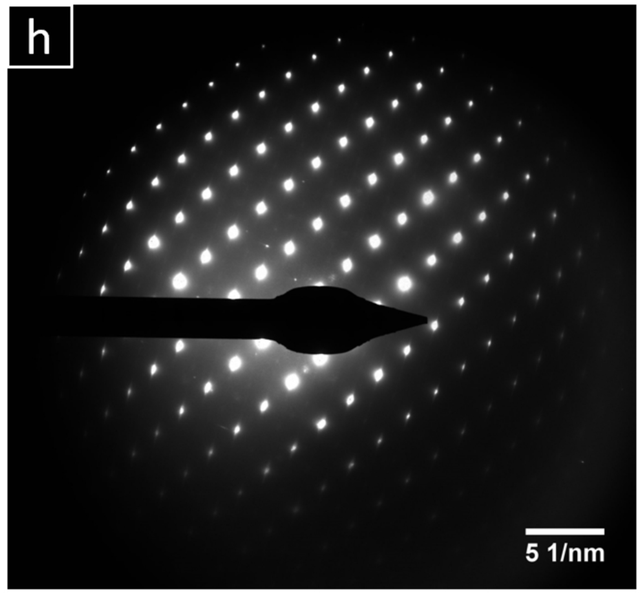

ACCEPTED MANUSCRIPT

Journal of Vacuum Science & Technology A

This is the author's peer reviewed, accepted manuscript. However, the online version of record will be different from this version once it has been copyedited and typeset.
PLEASE CITE THIS ARTICLE AS DOI: 10.1116/6.0000...

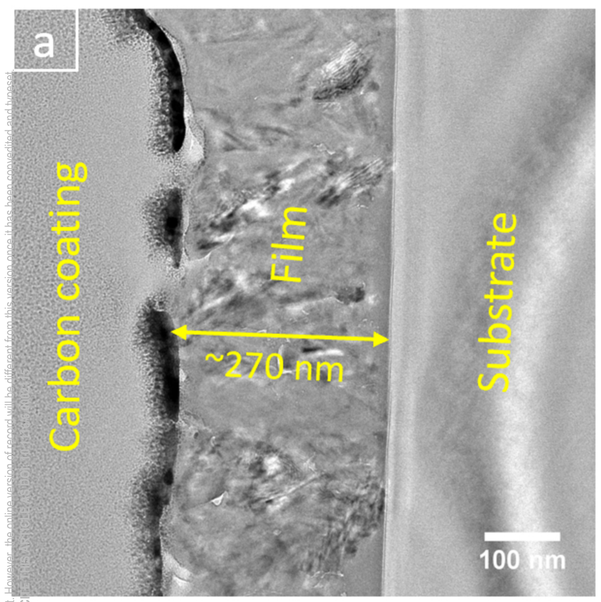

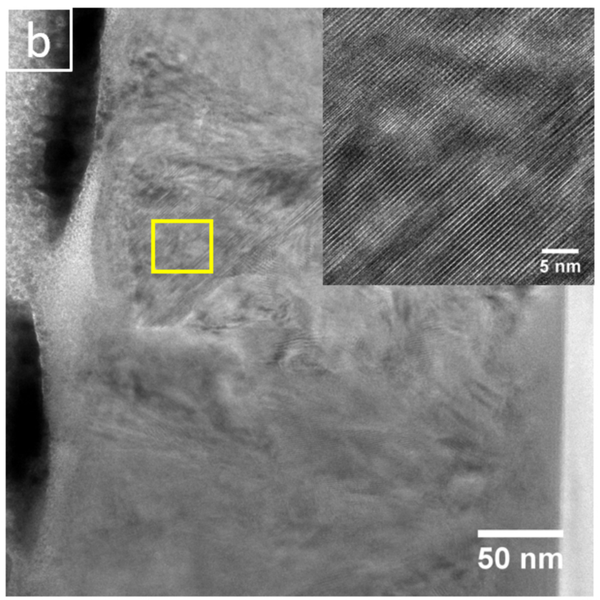

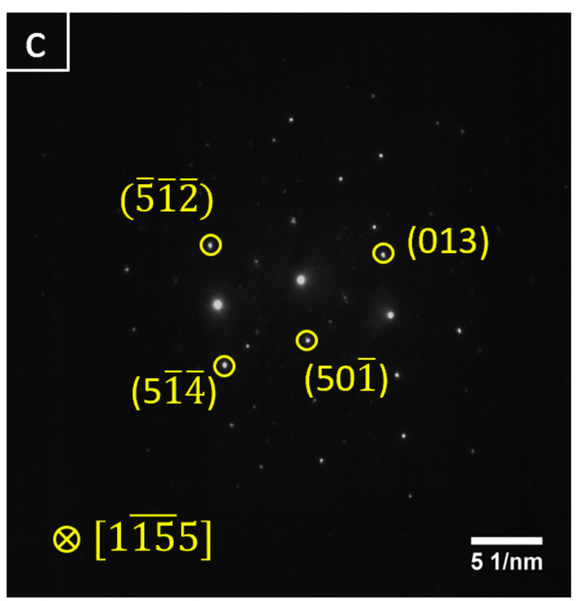

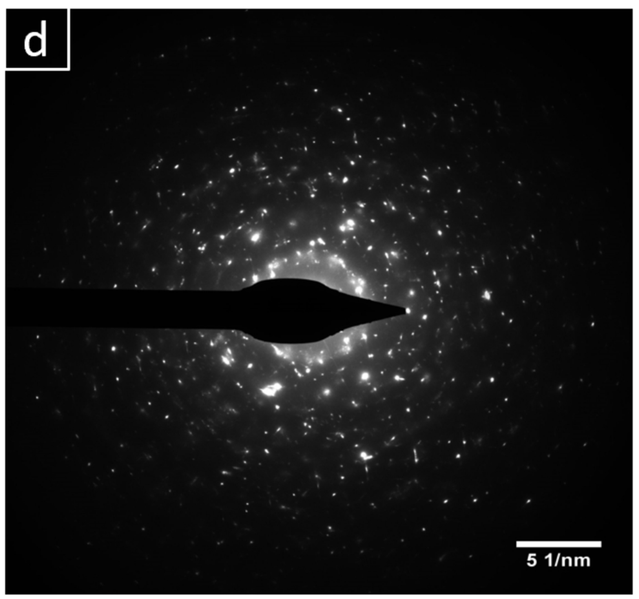

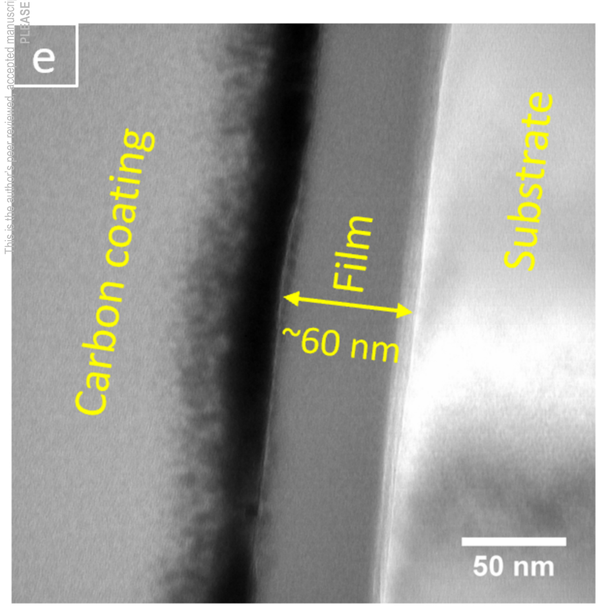

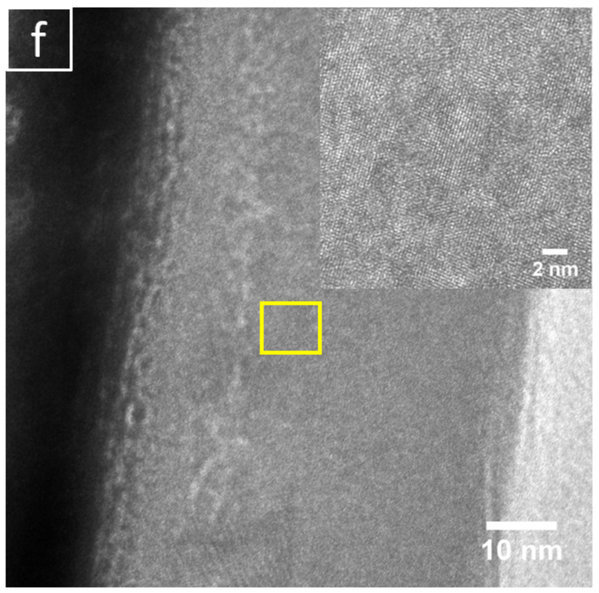

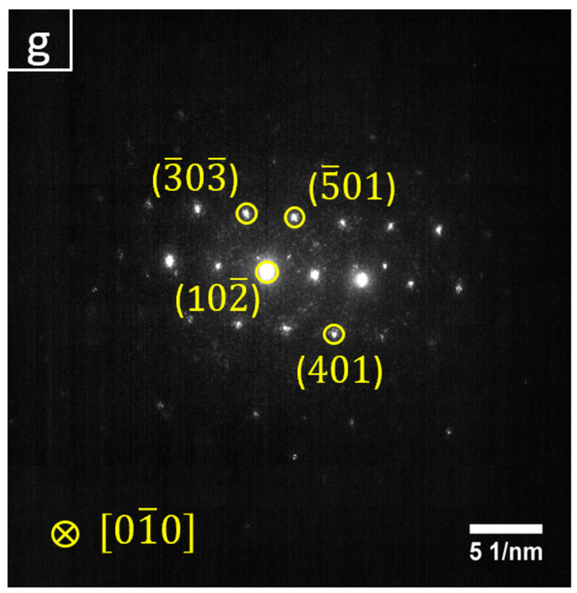

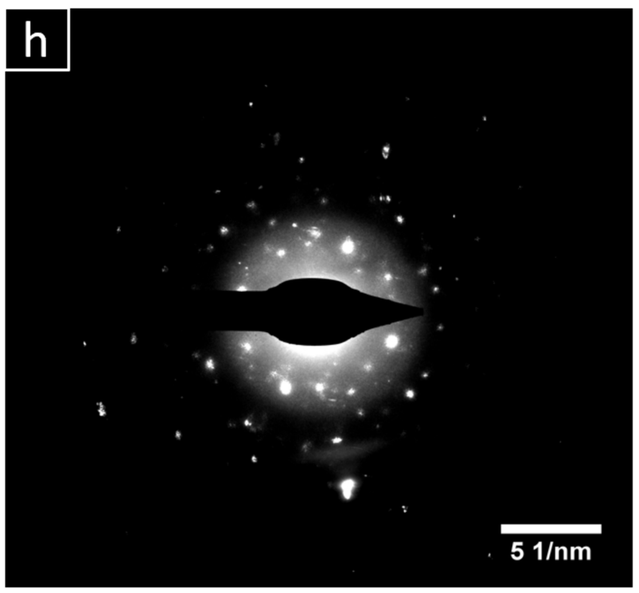

Journal of Vacuum Science & Technology A

ACCEPTED MANUSCRIPT

This is the author's peer reviewed, accepted manuscript. However, the online version of record will be different from this version once it has been copyedited and typeset.

PLEASE CITE THIS ARTICLE AS DOI: 10.1116/6.0002115

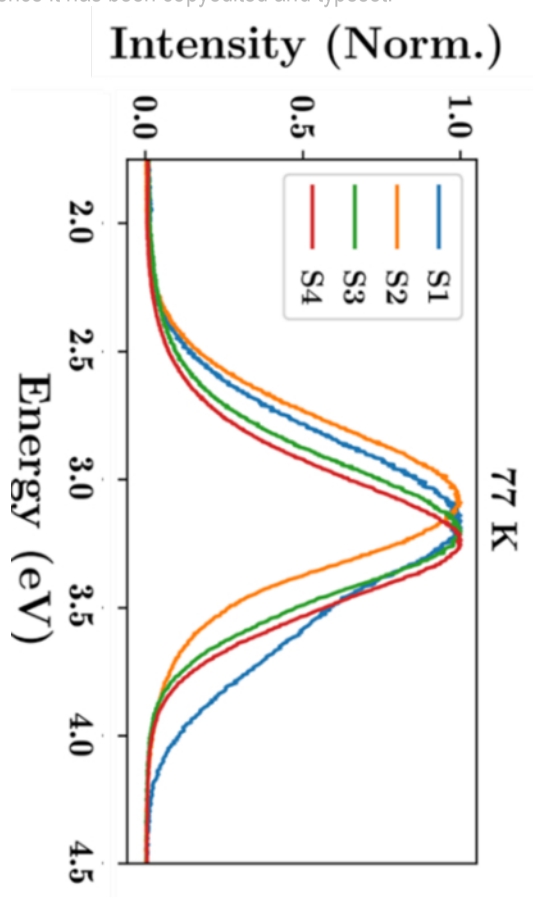

ACCEPTED MANUSCRIPT

Journal of Vacuum Science & Technology A

This is the author's peer reviewed, accepted manuscript. However, the online version of record will be different from this version once it has been copyedited and typeset.
PLEASE CITE THIS ARTICLE AS DOI: 10.1116/1.4921115

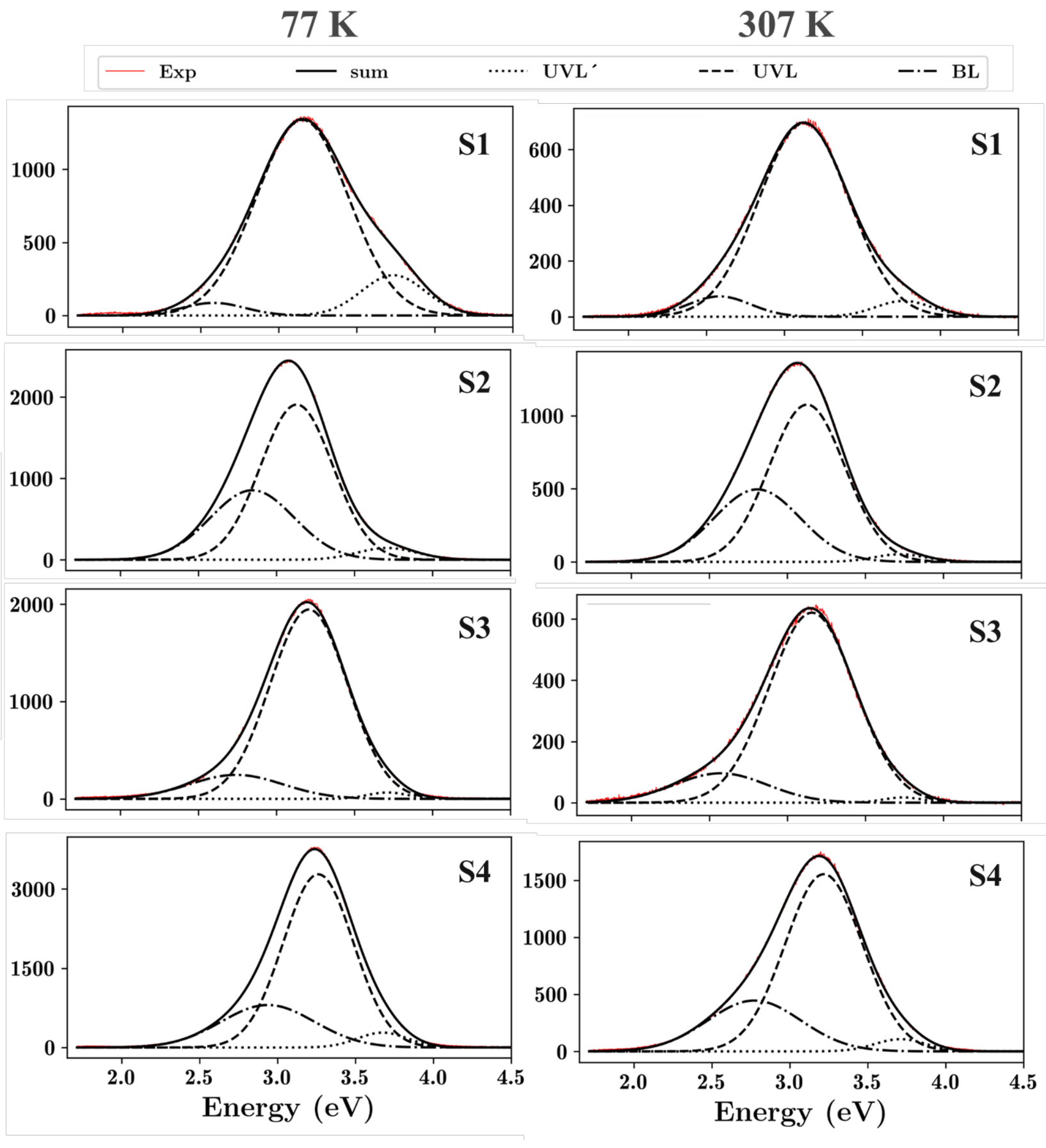

Journal of Vacuum Science & Technology A

ACCEPTED MANUSCRIPT

This is the author's peer reviewed, accepted manuscript. However, the online version of record will be different from this version once it has been copyedited and typeset.
PLEASE CITE THIS ARTICLE AS DOI: 10.1116/6.0002115

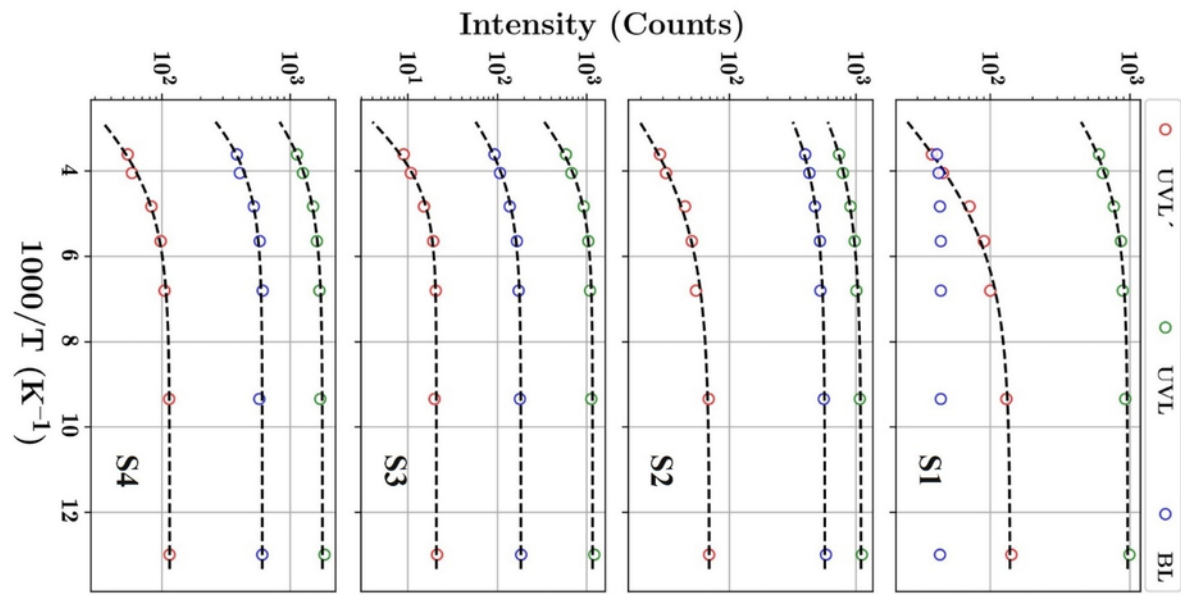

ACCEPTED MANUSCRIPT

Journal of Vacuum Science & Technology A

This is the author's peer reviewed, accepted manuscript. However, the online version of record will be different from this version once it has been copyedited and typeset.
PLEASE CITE THIS ARTICLE AS DOI: 10.1116/6.0002115